Tau pathology in cognitively normal older adults: Associations with brain atrophy and cognitive decline

Jacob Ziontz, BA[a,1], Murat Bilgel, PhD[a,1,*], Andrea T. Shafer, PhD[a], Abhay Moghekar, MD[f], Wendy Elkins, MS[a], Jessica Helphey BS[a], Gabriela Gomez, BS[a], Danielle June, BA[a], Michael A. McDonald, MD, PhD[c], Robert F. Dannals, PhD[c], Babak Behnam Azad, PhD[c], Luigi Ferrucci, MD, PhD[b], Dean F. Wong, MD, PhD[c,d,e,f], Susan M. Resnick, PhD[a]

[a] *Brain Aging and Behavior Section, Laboratory of Behavioral Neuroscience, National Institute on Aging, Baltimore, MD, USA*
[b] *Longitudinal Studies Section, Translational Gerontology Branch, National Institute on Aging, Baltimore, MD, USA*
[c] *Department of Radiology and Radiological Science, Johns Hopkins University School (JHU) of Medicine, Baltimore, MD, USA*
[d] *Department of Psychiatry and Behavioral Sciences, JHU School of Medicine, Baltimore, MD, USA*
[e] *Department of Neuroscience, JHU School of Medicine, Baltimore, MD, USA*
[f] *Department of Neurology, JHU School of Medicine, Baltimore, MD, USA*

Abstract

Introduction: Tau pathology, a hallmark of Alzheimer's disease, is observed in the brains of virtually all individuals over 70. Tau PET imaging enables the *in vivo* characterization of tau distribution and its effects on changes in brain volume and cognitive performance in cognitively normal older individuals.
Methods: Using ^{18}F-AV-1451 (^{18}F-flortaucipir) PET, we evaluated tau pathology in 54 cognitively normal participants (mean age 77.5, SD 8.9) from the Baltimore Longitudinal Study of Aging. We assessed associations between PET signal and age, sex, race, and amyloid positivity using voxel-wise linear regression. We further investigated associations between regional PET signal and retrospective longitudinal rates of change in regional volumes and domain-specific cognitive function using linear mixed effects models adjusting for age, sex, and amyloid status.
Results: Greater age, male sex, black race, and amyloid positivity were associated with higher ^{18}F-AV-1451 retention in distinct brain regions. Areas of likely tauopathy based on the intersection of associations with age and amyloid positivity were also identified. Adjusting for age, sex, and amyloid status, tracer retention in the entorhinal cortex was related to lower entorhinal volume ($\beta = -1.124, \text{SE} = 0.485, p = 0.025$) and a trend to steeper declines in hippocampal volume ($\beta = -0.061, \text{SE} = 0.032, p = 0.061$). Entorhinal ^{18}F-AV-1451 retention was also associated with steeper decline in memory performance ($\beta = -0.086, \text{SE} = 0.039, p = 0.029$), and signal in Braak III/IV regions was associated with steeper decline in verbal long-delay free recall ($\beta = -0.163, \text{SE} = 0.073, p = 0.026$).
Discussion: Entorhinal tau pathology is associated with declines in memory and medial temporal lobe volume even in cognitively normal individuals with low overall tau burden. The ability to assess medial temporal tau pathology will provide critical insights into early structural brain changes associated with later cognitive impairment and Alzheimer's disease.

Keywords: tau, AV-1451, T807, flortaucipir, FTP, PET, cognition, volume, longitudinal, cognitively normal

Abbreviations: AD, Alzheimer's disease; *APOE*, apolipoprotein E; BA, Brodmann area; BLSA, Baltimore Longitudinal Study of Aging; CN, cognitively normal; CSF, cerebrospinal fluid; CVLT, California Verbal Learning Test; DVR, distribution volume ratio; FWHM, full-width at half-maximum; HRRT, High Resolution Research Tomograph; ICV, intracranial volume; MCI, mild cognitive impairment; MPRAGE, magnetization-prepared rapid gradient echo; MRI, magnetic resonance imaging; MUSE, multi-atlas region segmentation using ensembles of registration algorithms and parameters; NFT, neurofibrillary tangle; PART, primary age-related tauopathy; PET, positron emission tomography; PiB, Pittsburgh compound B; RBV, region-based voxel-wise partial volume correction; ROI, region of interest; SD, standard deviation; SE, standard error; SUVR, standardized uptake value ratio.

*Corresponding author
Email address: murat.bilgel@nih.gov (Murat Bilgel, PhD)
URL: orcid.org/0000-0002-1995-3827 (Jacob Ziontz, BA), orcid.org/0000-0001-5042-7422 (Murat Bilgel, PhD), orcid.org/0000-0003-4599-5980 (Andrea T. Shafer, PhD)

[1] These authors contributed equally to this work.

1. Introduction

Pathological tau is a hallmark of several neurodegenerative diseases, the most prevalent of which is Alzheimer's disease (AD). Hyperphosphorylation of the tau protein, which normally promotes assembly and stability of microtubules in the nervous system [1], leads to the formation of neurofibrillary tangles (NFT). NFTs are observed at autopsy in brains of almost all individuals above 70 regardless of cognitive status, and tau burden correlates with brain atrophy and lower performance on neuropsychological testing prior to death [2]. NFTs in the entorhinal cortex and hippocampus in the absence of amyloid deposition and clinical symptomatology has been referred to as primary age-related tauopathy (PART) and is common in older adults [3]. However, there is currently no consensus as to whether PART is distinct from the continuum of AD [4], and a recent study from our group indicated that 47% of individuals aged ≥ 85 years with PART had cognitive impairment [5].

In preclinical AD, in which individuals exhibit AD neuropathology but remain cognitively normal (CN) [6], tau pathology is hypothesized to be one of the earliest pathophysiological changes [7], with tau spreading from the entorhinal cortex and hippocampus to the neocortex at later disease stages [8]. Given that the preclinical stages of AD are thought to present the best opportunity for intervention to prevent or mitigate neuronal and cognitive deterioration, it is important to understand how tau pathology in the earliest stages might modulate brain structure and cognition to better inform the development of therapeutics. In addition, understanding whether tau in the absence of amyloid deposition contributes to neurodegeneration and cognitive changes may provide insights into the optimal time frame for administering interventions aimed at modifying tau pathology.

The advent of tau radiotracers for positron emission tomography (PET) imaging has enabled the *in vivo* characterization of pathological tau, providing an important tool for understanding its correlates in aging and the earliest stages of preclinical AD. Several studies have investigated factors associated with tau PET signal, but most analyses include clinically impaired along with CN individuals, limiting the generalizability of these results. Cross-sectional studies including participants with mild cognitive impairment (MCI) or AD in addition to CN individuals have shown that higher temporal lobe tau PET signal is associated with lower memory performance [9, 10], and that lower hippocampal volume is associated with greater tau radiotracer retention in the same region [10, 11]. Pontecorvo and colleagues also reported associations between higher neocortical tau PET signal and greater cognitive impairment among amyloid positive individuals [12]. Longitudinal studies including individuals ranging from CN to demented have further found that higher baseline tau PET signal is associated with greater longitudinal rates of brain volume loss [13, 14] and global cognitive decline [15–17].

The scientific literature assessing the relationships of tau PET with cognition and brain volume in samples consisting only of CN individuals remains sparse. In a study of 30 CN older adults, adjusting for age, sex, and a continuous measure of overall brain amyloid burden, tau PET signal in a composite of the entorhinal cortex and hippocampus was associated with steeper longitudinal decline in episodic memory preceding PET as well as lower episodic memory at the time of PET [18]. A study of 133 clinically healthy older adults reported a cross-sectional association between entorhinal tau burden and subjective cognitive complaints, independent of amyloid pathology [19]. However, another study of 109 CN older individuals found no cross-sectional associations between regional tau PET signal and a composite cognitive score [20]. The association of tau PET signal with regional brain volume among CN participants is even less thoroughly explored. One cross-sectional study of 88 CN participants found negative local correlations between tau PET signal and gray matter volume intensity, especially in the inferior temporal gyrus and medial temporal lobe [21]. Moreover, these authors showed that tau PET signal in these areas also corresponded to widespread reduction in gray matter across the cortex.

Studying tau PET signal among CN individuals is challenging given that tau deposition is not as widespread in this population as in impaired individuals, and signal due to tau is relatively low and confounded by non-specific binding with current radiotracers [22, 23]. There is a need for further investigation of correlates of tau PET signal, particularly among CN individuals, to better distinguish specific from non-specific binding.

In this study, we first identified factors associated with tau PET signal in a sample of 54 CN older adults from the National Institute on Aging Baltimore Longitudinal Study of Aging (BLSA) using voxel-wise linear regression. We then characterized areas where tau PET signal is more likely to reflect the tau pathology present in preclinical AD, rather than non-specific binding, based on the associations of the signal with amyloid positivity and age. Finally, we examined the relationships between regional tracer retention and retrospective longitudinal measures of regional brain volume and cognitive performance. We hypothesized that age and amyloid positivity would be associated with tau PET signal given the relevance of these two factors

for AD progression. We also hypothesized that tau PET signal would explain retrospective brain volume loss in corresponding regions and cognitive decline in domains known to be affected early in AD, particularly memory.

2. Methods

2.1. Participants

The study sample included CN BLSA participants with a ^{18}F-AV-1451 (^{18}F-flortaucipir) tau PET, a ^{11}C-Pittsburgh compound B (^{11}C-PiB) amyloid PET within 2.2 years of tau PET, and a structural MRI. As of January 18, 2018, tau PET scans were acquired on 63 participants. Four had a non-CN status, two did not have an MRI at the time of analysis, one was subsequently discovered to have had an unreported myocardial infarction prior to enrollment (therefore meeting the exclusion criteria for PET study enrollment), and one was determined to be an outlier due to highly lateralized cortical signal. The final sample, after excluding these cases, consisted of 54 individuals (Table 1). For 47 of these participants, MRI and PET scans were ≤ 6 months apart. They were 0.6, 2.1, 2.1, 4.1, 4.6, 5.8, 7.3 years apart for the remaining 7 participants.

Normal cognitive status was based on either (i) a Clinical Dementia Rating score [24] of zero and ≤ 3 errors on the Blessed Information-Memory-Concentration Test [25], and therefore the participant did not meet criteria for consensus conference; or (ii) the participant met criteria for consensus conference and was determined to be CN based on thorough review of clinical and neuropsychological data.

Research protocols were approved by local institutional review boards, and all participants gave written informed consent at each visit. At enrollment into the PET neuroimaging substudy of the BLSA, all participants were free of CNS disease (dementia, stroke, bipolar illness, epilepsy), severe cardiac disease (one participant had a myocardial infarction and another was diagnosed with congestive heart failure after enrollment into the PET substudy but before tau PET scan), severe pulmonary disease, and metastatic cancer.

2.2. Structural imaging

Magnetization-prepared rapid gradient echo (MPRAGE) images were acquired on a 3 T Philips Achieva scanner (repetition time = 6.8 ms, echo time = 3.2 ms, flip angle = 8°, image matrix = 256×256, 170 slices, voxel size = $1 \times 1 \times 1.2$ mm). Anatomical labels and global and regional brain volumes were obtained using Multi-atlas region Segmentation using Ensembles of registration algorithms and parameters (MUSE) [26]. Regions of interest (ROI) included Braak I (entorhinal cortex), Braak II (hippocampus), Braak III/IV (composite of parahippocampal gyri, fusiform, lingual gyri, inferior and middle temporal gyri, posterior cingulate gyri, temporal pole, insula, amygdala, thalamus, and caudate), and Braak V/VI (precentral, superior frontal, postcentral gyri, cuneus). We performed intracranial volume (ICV) correction using the approach employed by Jack et al. [27], computing residual volumes for each ROI, which is the difference, in cm^3, from the regional volume that would be expected at a given intracranial volume.

2.3. Amyloid imaging

PET scans were obtained over 70 min on a GE Advance scanner immediately following an intravenous bolus injection of approximately 555 MBq (15 mCi) of ^{11}-C-PiB. Dynamic images were reconstructed using filtered back-projection with a ramp filter, yielding a spatial resolution of approximately 4.5 mm full-width at half-maximum (FWHM) at the center of the field of view (image matrix = 128×128, 35 slices, voxel size = $2 \times 2 \times 4.25$ mm). Each of the 33 time frames was aligned to the mean of the first 2 min to correct for motion using SPM's Realign (`https://www.fil.ion.ucl.ac.uk/spm/software/spm12/`) [28]. The average of the first 20 min of PET scans was rigidly registered onto the corresponding inhomogeneity-corrected MPRAGE, and the anatomical label image was transformed from MRI to PET space using FLIRT [29] implemented in FSL (`https://fsl.fmrib.ox.ac.uk/fsl`, version 6.0) [30]. Distribution volume ratio (DVR) images were computed in PET native space using a simplified reference tissue model [31] with cerebellar gray matter as the reference region. Mean cortical amyloid-β burden was calculated as the average of the DVR values in cingulate, frontal, parietal (including precuneus), lateral temporal, and lateral occipital cortical regions, excluding the sensorimotor strip. Individuals were categorized as amyloid −/+ based on a mean cortical DVR threshold of 1.057, which was derived from a Gaussian mixture model (Figure A.1).

Table 1: Participant demographics.

a. Voxel-wise analysis sample (n = 54)	**Amyloid− (n = 41)**	**Amyloid+ (n = 13)**
Age at ^{18}F-AV-1451 PET scan (yrs), mean (SD)	77.2 (8.9)	78.2 (9.3)
Male, n (%)	16 (39%)	8 (62%)
Black, n (%)	8 (20%)	4 (31%)
Yrs of education, mean (SD)	17.9 (2.1)	16.6 (2.2)
APOE ε4+, n (%)	11 (27%)	7 (54%)
b. Cognition sample (n = 53)	**Amyloid− (n = 40)**	**Amyloid+ (n = 13)**
Age at ^{18}F-AV-1451 PET scan (yrs), mean (SD)	77.6 (8.7)	78.2 (9.3)
Male, n (%)	16 (40%)	8 (62%)
Black, n (%)	8 (20%)	4 (31%)
Yrs of education, mean (SD)	17.8 (2.1)	16.6 (2.2)
APOE ε4+, n (%)	10 (25%)	7 (54%)
Number of cognitive assessments, mean (SD)	8 (5.2)	6.5 (5.5)
Duration of cognitive follow-up (yrs), mean (SD)	13.9 (8)	11.5 (8.7)
c. Brain volume sample (n = 50)	**Amyloid− (n = 38)**	**Amyloid+ (n = 12)**
Age at ^{18}F-AV-1451 PET scan (yrs), mean (SD)	77.3 (8.9)	77.8 (9.5)
Male, n (%)	15 (39%)	7 (58%)
Black, n (%)	8 (21%)	3 (25%)
Yrs of education, mean (SD)	17.9 (2.1)	16.7 (2.3)
APOE ε4+, n (%)	10 (26%)	6 (50%)
Number of MRI scans, mean (SD)	5.3 (4.9)	4.3 (4.6)
Duration of MRI follow-up (yrs), mean (SD)	7.4 (6.8)	6.2 (6.5)

2.4. Tau imaging

PET scans were obtained over 30 min on a Siemens High Resolution Research Tomograph (HRRT) scanner starting 75 mins after an intravenous bolus injection of approximately 370 MBq (10 mCi) of ^{18}F-AV-1451. Dynamic images were reconstructed using ordered subset expectation-maximization to yield 6 time frames of 5 mins each with approximately 2.5 mm FWHM at the center of the field of view (image matrix = 256×256, 207 slices, voxel size = $1.22 \times 1.22 \times 1.22$ mm). We aligned the time frames between 80–100 minutes to the first frame in this interval using SPM's Realign. The 20 min average PET image was registered onto the inhomogeneity-corrected MPRAGE using rigid registration with FLIRT. Anatomical labels defined in MRI space were transformed into PET space. The 20 min average PET image was partial volume corrected using the Region-Based Voxel-wise (RBV) method [32] implemented in the PETPVC toolbox (`https://github.com/UCL/PETPVC`, version 1.2.0-b) [33]. For the geometric matrix transfer step of RBV, we used 26 bilateral MUSE ROIs (see Appendix B). We computed standardized uptake value ratio (SUVR) images by dividing the partial volume corrected PET intensities by the mean within the inferior cerebellar gray matter, which was defined using the approach described by Baker et al. [34] based on the SUIT atlas [35]. Mean SUVR was calculated for each cortical ROI. SUVR images were mapped into MNI space using the warp computed from ANTs (`http://stnava.github.io/ANTs/`, version 2.1.0) [36] deformable registration of the corresponding MRIs to a study-specific MRI template, and smoothed with a Gaussian filter (FWHM = 6 mm) prior to statistical analysis. We computed the average SUVR in each Braak ROI. Braak II (hippocampus) SUVRs were excluded from analysis due to choroid plexus signal spillover (Lee et al., 2018). PET image processing steps were streamlined using `nipype` (`https://nipype.readthedocs.io/`, version 1.0.3) [37] in Python 3.6.5.

2.5. Neuropsychological testing

Cognitive domain scores were obtained for memory (California Verbal Learning Test (CVLT) [38] immediate and long-delay free recall), attention (Trail Making Test [39] Part A and Digit Span [40] Forward), executive function (Trail Making Test Part B and Digit Span Backward), language (Category [41] and Letter Fluency [42]), visuospatial processing (Card Rotations Test [43], Clock Drawing Test [44]), and processing speed (Digit Symbol Substitution Test) [40]. These scores were computed by first converting each test score to a z-score using the baseline mean and standard deviation, and then averaging the z-scores within each cognitive domain. Prior to computing the z-scores for Trail Making Test Parts A and B, the individual cognitive test scores (time to completion, in seconds) were log transformed and negated so that higher z-scores indicated less time to completion.

2.6. Statistical analysis

2.6.1. Factors associated with tau accumulation

We used multiple linear regression to assess the associations between demographics, amyloid positivity and voxel-wise ^{18}F-AV-1451 SUVR. Independent variables included age, sex, race, amyloid status, and age $\times$ amyloid status. Education was not included as a predictor because of its low variance in our sample. Each independent variable was mean-centered to facilitate interpretation of model results. Voxel-wise linear regression was conducted using SPM12. Statistical significance was based on two-tailed T-tests with $p < 0.001$ (uncorrected for multiple comparisons) and restricted to clusters of at least 400 voxels. Regression results were visualized as dual-coded images [45] using the `nanslice` package (`https://github.com/spinicist/nanslice`). MNI coordinates of peak voxels and local maxima within significant clusters were obtained using `atlasreader` [46]. We transformed these MNI coordinates into Talairach coordinates [47] using an in-house Python implementation of the coordinate look-up procedure implemented in BioImage Suite Web, which is based on a non-linear mapping between a digitized Talairach atlas and the MNI template [48]. We performed a 9 mm-wide cube range search using the Talairach Client (`http://www.talairach.org/client.html`) to obtain anatomical labels for each peak and subpeak. The label with the most hits in the cube was chosen as the corresponding anatomical label. For top hits that were not assigned a Brodmann area (BA) in the Talairach client output, if there was another hit with the same anatomical label as the top hit, we report their BA where applicable. All label and BA assignments were confirmed via visual inspection and corrected as necessary.

Given that voxel-wise analyses might be susceptible to inter-subject registration errors, we tested the relationship between these predictors and regional ^{18}F-AV-1451 SUVR means computed in native PET space to verify our voxel-wise findings. Six anatomical ROIs were selected based on the observed voxel-wise effects and these effects were corroborated using a native space ROI approach (see Appendix C).

To identify voxels where ^{18}F-AV-1451 PET signal likely reflects preclinical AD-related tau pathology rather than non-specific binding in our sample of CN older adults, we created a conjunction map of the statistically significant voxels for three different effects in our model. First, we restricted the map to voxels with a positive effect of amyloid status given that amyloid accumulation is thought to be the earliest detectable brain change in preclinical AD [6, 7]. Next, we restricted the map to voxels with a positive age effect based on the hypothesis that tau accumulates with age in preclinical AD [49]. Lastly, given that we were interested in areas of greater age-related tau increase in amyloid positive individuals, we restricted the map to voxels where slope between age and tau PET signal differed by amyloid group (i.e., the positive age $\times$ amyloid group interaction term). The resulting conjunction map thus includes only voxels where (1) the age association with tau PET signal is stronger among amyloid positive versus negative individuals, (2) tau PET signal increases with age, and (3) where tau PET signal is greater in amyloid positive versus negative individuals. $p < 0.05$ was used to threshold each individual map and an extent threshold of 400 voxels was applied to the conjunction map. Results were visualized in a 'glass brain' format using `nilearn` [50] in Python 3.7.2. All of these steps were streamlined using the `nipype` package [37].

2.6.2. Longitudinal regional brain volume change and co-localized tau accumulation

We assessed associations between regional ^{18}F-AV-1451 SUVR and retrospective change in the volume of the same region using separate linear mixed effects models for each Braak ROI. The dependent variable was ICV-adjusted regional volumes prior to and concurrent with the tau PET scans. Age at and time from tau PET scan, sex, amyloid status (+ vs −), amyloid status $\times$ time, regional ^{18}F-AV-1451 SUVR, and

SUVR × time were included as independent variables. To facilitate interpretation, regional ^{18}F-AV-1451 SUVRs were mean-centered. Random effects were included for intercept and time. This analysis was restricted to individuals who had a volumetric measurement prior to and within 3 years of tau PET (n = 50, total number of longitudinal MRI assessments = 253). Additionally, we conducted analyses using ICV-adjusted bilateral hippocampal volume and bilateral entorhinal cortex volume as the dependent variable rather than corresponding regional volume given the relevance of volume change in these regions to preclinical AD [21].

2.6.3. Longitudinal cognition and tau accumulation

We assessed associations between ^{18}F-AV-1451 SUVR and retrospective change in cognition using linear mixed effects models with age at and time from tau PET scan, sex, years of education, amyloid status, amyloid status × time interaction, regional ^{18}F-AV-1451 SUVR, and regional SUVR × time interaction as independent variables. This analysis was restricted to individuals who had a cognitive assessment prior to and within 3 years of tau PET (n = 53). Across the 53 participants meeting this criterion, there were 401 total observations for memory, 351 for attention and executive function, 363 for language, 293 for visuospatial processing, and 249 for processing speed, with differences in sample sizes primarily reflecting historical differences in age at which specific tests were administered. Cognitive performance in memory, attention, executive function, language, visuospatial processing, and processing speed were each considered as a dependent variable in separate analyses. Amyloid status and regional ^{18}F-AV-1451 SUVRs were centered around the sample mean as before. Random effects were included for intercept and time. We used the `nlme` [51] package in R (`https://cran.r-project.org`, version 3.5.1) to fit the linear mixed effects models.

2.7. Computational reproducibility

PET image processing steps to generate SUVR images and all statistical analyses were containerized using Singularity [52] to ensure computational reproducibility. To compile this manuscript, we used the following R packages: `knitr` [53, 54] to generate this manuscript directly incorporating results from R, `kableExtra` [55] to format tables, `stargazer` [56] to tabulate model results, `ggplot2` [57] to generate the scatter and trajectory plots, and `ggpubr` [58] to create panel figures. Code for replicating the statistical analyses and producing this manuscript (except for manual edits in peak tables) is provided at `https://gitlab.com/bilgelm/tau_predictors`, and the Singularity image containing all necessary software at `https://www.singularity-hub.org/collections/2612`.

Data used in these analyses are available upon request from the BLSA website (`https://www.blsa.nih.gov`). All requests are reviewed by the BLSA Data Sharing Proposal Review Committee and are also subject to approval from the NIH IRB.

3. Results

3.1. Factors associated with tau accumulation

The association between age and ^{18}F-AV-1451 SUVR was stronger among amyloid positive compared to negative individuals in the right middle temporal gyrus, left middle frontal gyrus, and bilaterally in the cuneus, cingulate, superior frontal, and postcentral gyri (Table D.1). There were no regions where the association between age and ^{18}F-AV-1451 SUVR was stronger in the amyloid negative group. In the amyloid positive group, greater age was associated with higher ^{18}F-AV-1451 SUVR in bilateral putamen, right inferior frontal, and right middle occipital gyri (Table D.2). In the amyloid negative group, greater age was associated with lower ^{18}F-AV-1451 SUVR particularly in sulcal cerebrospinal fluid, ventricular, and periventricular areas (Table D.3). There were no regions in the amyloid positive group where lower SUVR was associated with higher age, and no regions in the amyloid negative group where higher SUVR was associated with higher age. There was a main effect of amyloid status in right middle frontal gyrus, right superior and middle temporal gyri, left superior occipital gyrus, and bilateral middle temporal gyri, middle occipital gyri and cuneus (Table D.4), such that positive individuals had greater ^{18}F-AV-1451 signal compared to negative individuals. There were no regions that showed greater ^{18}F-AV-1451 signal for amyloid negative relative to positive individuals. Men compared with women had higher ^{18}F-AV-1451 SUVR in bilateral frontal, parietal, and lateral temporal cortices as well as in bilateral limbic areas (Table D.5). There were no regions where females had greater ^{18}F-AV-1451 signal compared to men. Finally, black race was associated with higher ^{18}F-AV-1451 SUVR in bilateral occipital and temporal lobes as well as superior frontal areas (Table D.6).

These effects are visualized for select brain slices in Figure 1. Unthresholded statistical maps and corresponding imaging files from SPM output are available in NeuroImaging Data Model (NIDM)-Results format [59] at `https://neurovault.org/collections/LGNABWKB` [60].

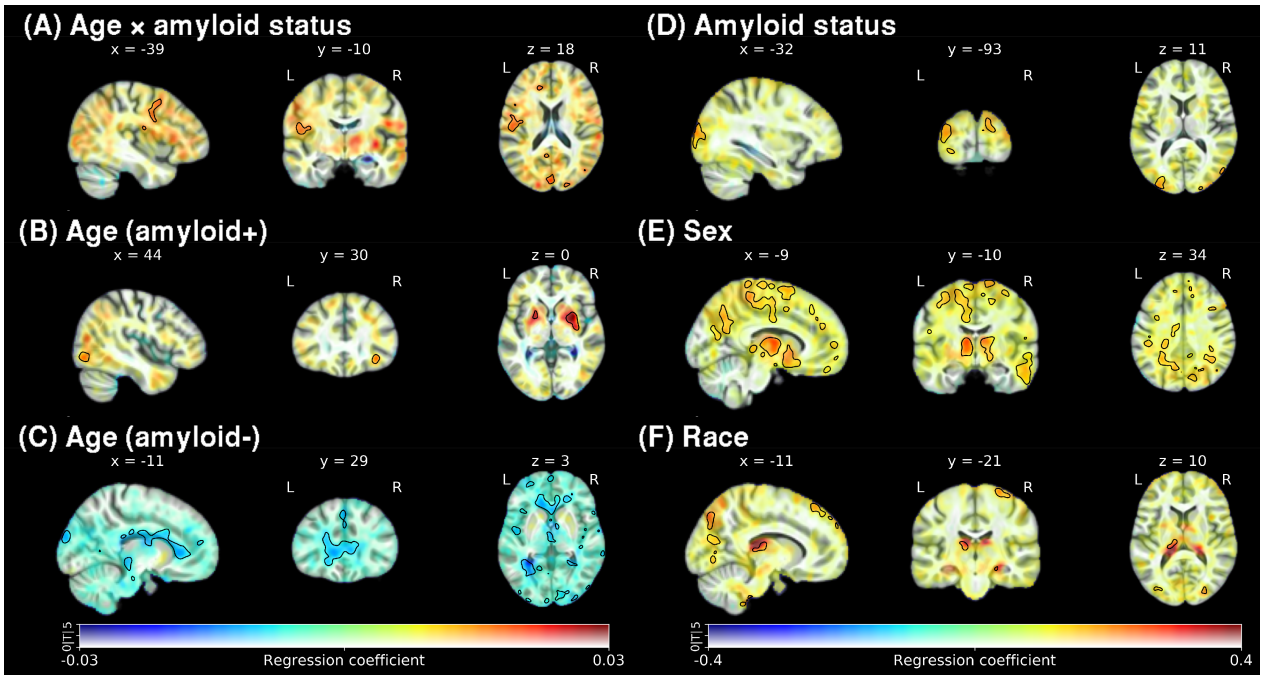

Figure 1: Predictors of ^{18}F-AV-1451 tau PET signal among cognitively normal older adults. In these dual-coded representations of voxel-wise linear regression results, color indicates the estimated regression coefficient and transparency corresponds to the absolute T-value (with 0 as completely transparent and ≥ 5 as completely opaque). Voxels that reach significance (uncorrected $p < 0.001$, cluster size ≥ 400 voxels) are circumscribed by black contour. (A) Age by amyloid status interaction. (B) Main effect of age in amyloid positive individuals. (C) Main effect of age in amyloid negative individuals. (D) Main effect of amyloid positivity. (E) Main effect of male sex. (F) Main effect of black race. Color bars on the left and right correspond to panels A–C and D–F, respectively.

Voxels showing higher ^{18}F-AV-1451 SUVR in amyloid positive individuals, a positive age effect in the amyloid positive group, and a significant age × amyloid group interaction comprised bilateral superior and middle frontal, superior and middle temporal, parahippocampal, and middle occipital gyri (Table 4). The resulting conjunction map aimed at identifying areas where ^{18}F-AV-1451 SUVR likely reflects preclinical AD tau pathology is shown in Figure 2.

3.2. Regional brain volume and tau accumulation

Cross-sectionally, higher entorhinal cortex ^{18}F-AV-1451 SUVR was associated with smaller volume in this region ($\beta = -1.124, \text{SE} = 0.485, p = 0.025$) (Table 2). Greater ^{18}F-AV-1451 SUVR in Braak III/IV was also associated with smaller regional volume in the entorhinal cortex ($\beta = -1.634, \text{SE} = 0.804, p = 0.049$) (Table E.1). In addition, greater ^{18}F-AV-1451 SUVR in the entorhinal cortex was associated with a trend to steeper longitudinal decline in hippocampal volume ($\beta = -0.061, \text{SE} = 0.032, p = 0.061$) (Table 2).

3.3. Cognition and tau accumulation

Lower attention scores were cross-sectionally associated with greater ^{18}F-AV-1451 SUVR in Braak III/IV ($\beta = -2.463, \text{SE} = 1.121, p = 0.033$) (Table F.1) as well as in Braak V/VI ($\beta = -2.033, \text{SE} = 0.885, p = 0.027$) (Table F.2).

Steeper decline in the memory score was associated with greater ^{18}F-AV-1451 SUVR in the entorhinal cortex ($\beta = -0.086, \text{SE} = 0.039, p = 0.029$) (Figure 3, Table 3). The strength of this association was greater for the CVLT long-delay free recall component ($\beta = -0.095, \text{SE} = 0.042, p = 0.024$) than for the immediate recall component ($\beta = -0.078, \text{SE} = 0.041, p = 0.06$) (Table F.3). Higher Braak III/IV SUVR was also

Figure 2: Conjunction map representing where ^{18}F-AV-1451 tau PET signal likely reflects areas of accumulating tau pathology in cognitively normal older adults. (A) Glass brain visualization of voxels where amyloid positive individuals have greater signal than amyloid negative individuals, where tracer signal is positively correlated with age among amyloid positive individuals, and where the age association is stronger among amyloid positive compared to amyloid negative individuals. Each component is thresholded at uncorrected $p < 0.05$ and cluster size ≥ 400 voxels. (B) Scatter plot of mean ^{18}F-AV-1451 SUVR extracted from the conjunction map mask vs. age. Amyloid positive individuals exhibit a positive association between age and tracer signal and higher overall tracer signal than amyloid negative individuals.

Table 2: Linear mixed effects models of the relationship between entorhinal ^{18}F-AV-1451 SUVR and intracranial volume adjusted regional volume in the entorhinal cortex and hippocampus. Estimated fixed effects are reported along with their standard errors in parentheses.

	Dependent variable: Regional volume (cm^3)	
	Entorhinal volume	Hippocampal volume
Intercept	−0.301*** (0.063)	−0.338*** (0.073)
	p = 0.000004	p = 0.00001
Age at PET scan	−0.030*** (0.007)	−0.045*** (0.008)
	p = 0.0002	p = 0.000003
Sex	0.338* (0.129)	0.383* (0.148)
(ref = female)	p = 0.013	p = 0.014
Amyloid group	0.231 (0.152)	−0.108 (0.175)
(ref = amyloid–)	p = 0.136	p = 0.541
Entorhinal SUVR	−1.124* (0.485)	−0.474 (0.562)
	p = 0.025	p = 0.404
Time from PET	−0.055*** (0.007)	−0.046*** (0.005)
	p = 0.000	p = 0.000
Amyloid group	−0.001 (0.017)	0.013 (0.012)
× time	p = 0.960	p = 0.267
Entorhinal SUVR	−0.047 (0.046)	−0.061 (0.032)
× time	p = 0.308	p = 0.061
Note:		*p<0.05; **p<0.01; ***p<0.001

associated with steeper declines in CVLT long-delay free recall ($\beta = -0.163, \text{SE} = 0.073, p = 0.026$), but not immediate recall ($\beta = -0.091, \text{SE} = 0.074, p = 0.22$) (Table F.4).

Table 3: Linear mixed effects models of the relationship between entorhinal ^{18}F-AV-1451 SUVR and cognition. Estimated fixed effects are reported along with their standard errors in parentheses.

	Dependent variable: Cognitive testing performance (z-score)					
	Memory	Attention	Executive Function	Language	Visuospatial Processing	Processing Speed
Intercept	0.126 (0.125) p = 0.312	0.119 (0.095) p = 0.213	0.014 (0.099) p = 0.891	0.062 (0.125) p = 0.619	−0.049 (0.092) p = 0.597	0.019 (0.117) p = 0.869
Age at PET scan	−0.029* (0.012) p = 0.021	−0.023* (0.011) p = 0.037	−0.021 (0.011) p = 0.058	−0.028* (0.013) p = 0.038	−0.022* (0.010) p = 0.030	−0.055*** (0.013) p = 0.0001
Sex (ref = female)	−0.082 (0.217) p = 0.708	−0.185 (0.188) p = 0.331	−0.064 (0.195) p = 0.745	0.022 (0.239) p = 0.928	0.151 (0.163) p = 0.361	−0.450 (0.230) p = 0.057
Education (years)	−0.066 (0.051) p = 0.205	0.016 (0.045) p = 0.717	−0.006 (0.046) p = 0.896	−0.052 (0.056) p = 0.354	−0.005 (0.038) p = 0.889	0.148** (0.055) p = 0.010
Amyloid group (ref = amyloid–)	0.131 (0.308) p = 0.673	0.118 (0.238) p = 0.623	−0.294 (0.247) p = 0.241	−0.137 (0.310) p = 0.661	0.030 (0.226) p = 0.896	0.021 (0.291) p = 0.943
Entorhinal SUVR	−0.769 (0.942) p = 0.419	−0.951 (0.714) p = 0.190	0.321 (0.746) p = 0.670	−0.503 (0.946) p = 0.598	0.399 (0.688) p = 0.565	−0.242 (0.885) p = 0.786
Time from PET	−0.023*** (0.006) p = 0.0001	−0.020*** (0.006) p = 0.001	−0.016*** (0.004) p = 0.0004	−0.011* (0.005) p = 0.016	−0.024*** (0.005) p = 0.000002	−0.097*** (0.010) p = 0.000
Amyloid group × time	0.007 (0.014) p = 0.646	−0.016 (0.015) p = 0.271	−0.019 (0.010) p = 0.056	0.023* (0.011) p = 0.047	0.006 (0.011) p = 0.588	−0.038 (0.026) p = 0.147
Entorhinal SUVR × time	−0.086* (0.039) p = 0.029	0.017 (0.033) p = 0.611	0.035 (0.023) p = 0.128	−0.037 (0.026) p = 0.161	0.045 (0.027) p = 0.095	−0.001 (0.073) p = 0.988
Note:						*p<0.05; **p<0.01; ***p<0.001

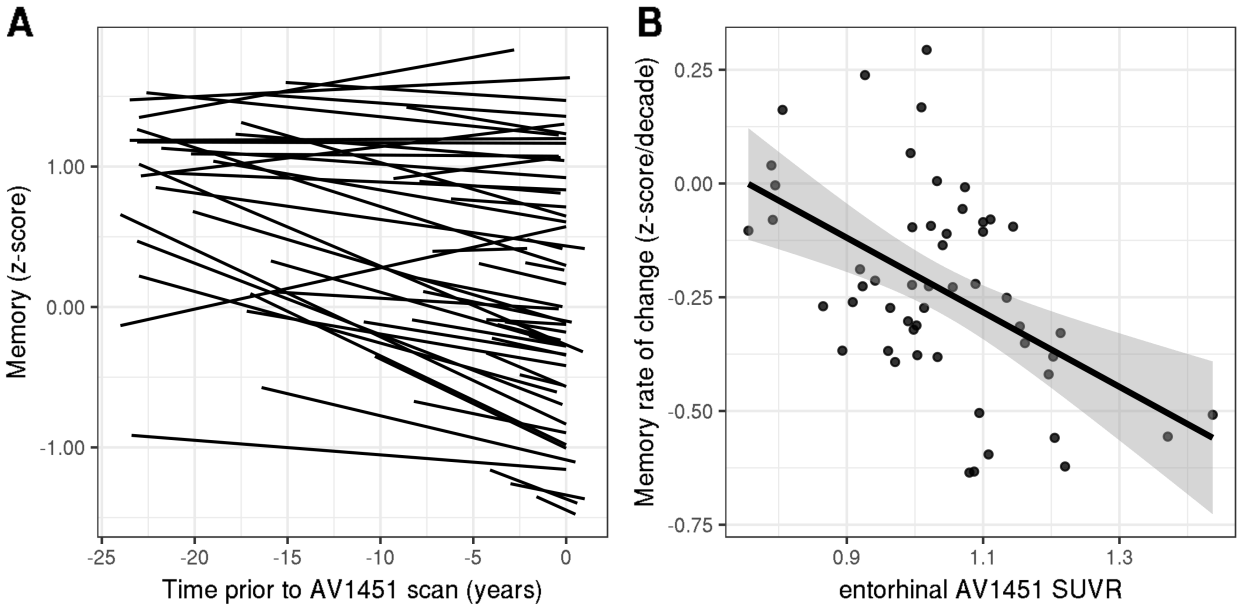

Figure 3: Entorhinal ^{18}F-AV-1451 tau PET signal is associated with steeper retrospective longitudinal decline in the composite memory score. (A) Individual-level memory change predicted by linear mixed effects model. (B) Rate of decline (z-score/decade) in memory performance as a function of ^{18}F-AV-1451 tau PET signal in the entorhinal cortex. Fitted values for rate of change are plotted for each individual in the sample.

Table 4: Peaks and subpeaks in the age × amyloid interaction term T-value map restricted to the conjunction mask. We also report the T-values for the age and amyloid group terms at these coordinates.

Label	Volume (mm^3)	MNI (x, y, z)	T-value		
			age × amyloid	age	amyloid
Bilateral					
Parietal, Cingulate					
R Precuneus BA 31	2093	(8, -63, 31)	4.01	2.63	2.01
L Cingulate Gyrus BA 31		(-3, -48, 27)	3.58	2.11	2.25
R Cingulate Gyrus BA 31		(12, -52, 25)	3.83	3.49	2.60
Left hemisphere					
Cingulate					
Anterior Cingulate BA 32	746	(-15, 35, 17)	4.24	2.52	2.05
Frontal					
Inferior Frontal Gyrus BA 44	1042	(-47, 10, 11)	4.63	3.75	3.15
Precentral Gyrus BA 4		(-52, 5, -1)	4.66	2.22	2.14
Middle Frontal Gyrus BA 10	415	(-34, 50, 8)	4.20	2.88	2.55
Middle Frontal Gyrus BA 6	1661	(-42, 4, 46)	5.09	4.36	2.62
Precentral Gyrus BA 6		(-51, -4, 45)	3.73	3.07	2.42
Superior Frontal Gyrus BA 8		(-36, 17, 52)	2.82	2.26	3.15
Superior Frontal Gyrus BA 9	515	(-15, 37, 42)	4.29	3.65	2.23
Occipital					
Cuneus BA 18	479	(0, -87, 18)	5.13	3.83	2.11
Parietal					
Angular Gyrus BA 39		(-47, -63, 30)	4.39	3.24	2.30

	849				
Inferior Parietal Lobule BA 40		(-41, -57, 45)	2.82	2.08	2.28
Parietal Sub-Gyral	475	(-24, -61, 34)	3.96	2.94	2.04
Postcentral Gyrus BA 43	1184	(-52, -15, 19)	4.56	3.24	3.29
Temporal					
Fusiform Gyrus BA 20/37	1073	(-30, -42, -23)	2.90	2.65	2.05
Parahippocampal Gyrus BA 36		(-28, -48, -12)	3.52	2.79	2.11
Temporal, Occipital					
Middle Temporal Gyrus	7774	(-33, -71, 19)	4.15	3.19	2.79
Middle Temporal Gyrus BA 39		(-45, -70, 10)	3.06	2.26	2.08
Inferior Occipital Gyrus BA 19		(-41, -87, 1)	4.08	2.52	2.24
Lingual Gyrus BA 18		(-17, -80, -11)	4.02	3.73	2.26
Lingual Gyrus BA 19		(-26, -71, -8)	3.80	2.63	2.11
Middle Occipital Gyrus BA 18		(-27, -94, 9)	3.93	2.67	3.38
Superior Occipital Gyrus BA 19		(-35, -83, 24)	4.07	3.41	2.99
Right hemisphere					
Frontal					
Frontal Sub-Gyral	663	(34, 26, 13)	4.69	4.28	2.08
Inferior Frontal Gyrus BA 47		(44, 28, 5)	3.22	2.32	2.19
Middle Frontal Gyrus BA 9		(31, 30, 31)	3.16	2.98	2.04
Superior Frontal Gyrus BA 6	442	(14, 8, 66)	3.33	2.25	2.25
Frontal, Subcortical					
Insula BA 13	3168	(37, 10, -7)	3.68	2.91	2.13
Lateral Globus Pallidus		(13, 5, -2)	2.54	3.09	2.08
Lateral Putamen		(32, 6, 6)	3.83	4.27	2.02
Parietal, Temporal					
Supramarginal Gyrus BA 40	1346	(49, -52, 35)	3.83	2.84	2.22
Superior Temporal Gyrus BA 39		(52, -62, 26)	4.06	3.03	3.21
Temporal					
Inferior Temporal Gyrus BA 20	3457	(46, 1, -40)	3.70	3.88	2.54
Middle Temporal Gyrus BA 20		(44, 8, -29)	3.85	3.59	2.61
Middle Temporal Gyrus BA 21		(58, -6, -25)	3.64	3.12	2.25
Inferior Temporal Gyrus BA 20	652	(50, -21, -24)	2.50	2.15	3.48
Superior Temporal Gyrus BA 42	785	(61, -30, 16)	4.41	2.80	2.03
Temporal, Occipital					
Fusiform Gyrus BA 19	13353	(32, -48, -12)	2.79	2.28	2.45
Fusiform Gyrus BA 37		(43, -41, -17)	2.62	2.46	2.12
Middle Temporal Gyrus BA 21		(65, -20, -14)	3.99	3.78	2.07
Middle Temporal Gyrus BA 22		(62, -36, -5)	3.65	3.57	2.03
Middle Temporal Gyrus BA 37		(56, -47, -16)	4.58	4.29	2.49
Middle Temporal Gyrus BA 39		(43, -71, 14)	4.12	3.75	2.04
Superior Temporal Gyrus BA 22		(56, -50, 10)	3.24	2.72	2.95
Middle Occipital Gyrus BA 19		(45, -77, -8)	5.21	5.75	4.15

Abbreviations:
BA = Brodmann area, L = Left, R = Right.

4. Discussion

Our study investigated tau PET signal among cognitively normal individuals. We evaluated the cross-sectional associations of ^{18}F-AV-1451 SUVR with age, sex, race, and amyloid status. Given that AV-1451 exhibits non-specific binding [61] and that SUVR measures are confounded by blood flow effects [62], we sought

to identify brain areas where ^{18}F-AV-1451 SUVR is more likely to reflect specific binding to phosphorylated tau. To this end, we employed a conjunction map approach guided by the current hypotheses in preclinical AD research that the presence of amyloid enables, is a risk factor for, or is a biomarker of the spread of tau pathology into the neocortex [63], and that tau pathology becomes more prevalent with age. Through this conjunction map, we identified the parahippocampal, superior and middle temporal, superior and middle frontal, and middle occipital gyri as the main areas of ^{18}F-AV-1451 retention that are likely to reflect tau pathology among cognitively normal individuals with elevated levels of amyloid deposition. Finally, we assessed the associations between ^{18}F-AV-1451 SUVR and rates of volumetric and cognitive change and found that higher entorhinal ^{18}F-AV-1451 retention was associated with steeper decline in verbal memory and a trend to steeper decline in hippocampal volume.

Our finding of higher ^{18}F-AV-1451 SUVR in temporal, temporoparietal, and frontal cortical areas among amyloid+ compared to amyloid– individuals is in agreement with previous studies of cognitively normal older adults [18, 49]. In amyloid negative individuals, we found that ^{18}F-AV-1451 SUVR was lower at greater ages, largely confined to periventricular white matter and sulcal CSF which are regions of suspected non-specific tracer signal. Conversely, ^{18}F-AV-1451 SUVR was higher at older ages among amyloid positive individuals in the putamen, right inferior frontal, and right middle occipital gyri. The association between tracer retention and age modulated by amyloid status did not reach significance in the putamen, but amyloid positive individuals exhibited stronger associations in several cortical regions. These findings suggest that the association in the putamen may be driven by non-specific binding whereas cortical associations may more likely be due to tau pathology. Similarly, the observed interaction between amyloid status and age might be reflective of cortical areas of faster tau accumulation among amyloid positive individuals. This interpretation is supported by the finding of a previous longitudinal tau PET study showing that amyloid positive individuals had steeper tau PET signal increases in basal and mid-temporal, retrosplenial, posterior cingulate, and entorhinal cortex [64]. Another study of longitudinal tau accumulation showed increases in ^{18}F-AV-1451 retention over 1–3 years in temporal and medial parietal areas in healthy older adults [65], in agreement with the regions identified in our conjunction map. In another recent study, individuals with baseline ^{18}F-AV-1451 SUVR in the second quartile exhibited increases over 18 months in inferior and lateral temporal cortex and in posterior cingulate [17].

Men in our sample had higher ^{18}F-AV-1451 SUVR than women, mainly in frontal and parietal white matter and thalamus, areas that were not included in our conjunction map. Previous studies utilizing tau PET imaging have not shown widespread or consistent sex differences in tracer retention [49, 66], and given that women exhibit a greater degree of AD pathology than men in *ex vivo* measures of tau [67], it seems likely that the sex differences we observed are largely driven by non-specific binding of the radiotracer. Additionally, we found higher ^{18}F-AV-1451 SUVR among black individuals in confined regions of the cortex. Black individuals exhibit lower levels of CSF-tau than white individuals [68], but greater incidence of postmortem NFT in Braak V/VI in black individuals has also been observed[69]. Race-related differences in ^{18}F-AV-1451 retention in the choroid plexus have been previously reported [70], but the proximity of most statistically significant clusters to the edge of the brain in our sample suggests that these findings may be in part due to spill-over from non-specific meningeal binding of the tracer. Potential sex and race differences in tau deposition will require further study in large and diverse samples.

Adjusting for age, sex, and amyloid status, we found that higher entorhinal ^{18}F-AV-1451 SUVR was associated with lower brain volume in this region and with a trend to greater rate of decline in hippocampal volume. These findings suggest that tau accumulation may help explain differences in regional volume in certain brain areas, as well as variation in volume changes in areas relevant for cognitive processes affected in AD. Previous studies of the relationship between PET tau and brain atrophy have reported more extensive associations between tau pathology and regional volume. Iaccarino et al. [14] observed that greater ^{18}F-AV-1451 SUVR was associated with lower gray matter volume cross-sectionally in anterior frontal and posterior occipital areas. Das et al. [13] also found that greater medial temporal lobe ^{18}F-AV-1451 SUVR was associated with both cross-sectional cortical thickness and rate of thickness change in amyloid positive individuals. Notably, these studies utilized cohorts that included both MCI and AD individuals as well as healthy controls. The absence of a widespread association between ^{18}F-AV-1451 SUVR and brain volume change in our sample suggests that associations between tau pathology and neurodegeneration are modest in cognitively normal individuals with low overall tau burden, but become more pronounced with the onset of symptomatic disease and cognitive impairment.

Adjusting for age, sex, education, and amyloid status, we observed that greater ^{18}F-AV-1451 retention in the entorhinal cortex and in Braak III/IV regions was associated with steeper decline in verbal memory performance. This finding in cognitively normal individuals reinforces the notion that tau accumulation in areas associated with the earliest pathological burden may influence changes in cognitive domains known to be affected in AD. We had found an association between amyloid status and steeper memory decline in a previous analysis using the BLSA amyloid PET data [71]. Interestingly, this association was not statistically significant in our current analyses including entorhinal ^{18}F-AV-1451 SUVR as an independent variable. This suggests that tau rather than amyloid deposition may be more strongly associated with cognition, consistent with previous findings [9]. Retention in Braak III/IV as well as Braak V/VI regions was also associated cross-sectionally with worse performance in the attention domain, an unexpected finding that requires replication. Other studies have reported a relationship between tau burden and performance in multiple cognitive domains [15, 72], but these findings were likely driven by the clinically-impaired individuals included in the sample.

AD pathology has long been considered to influence cognition via its effects on neuronal integrity and brain atrophy. Pathological amyloid and tau together at the synapse have been associated with altered calcium signaling, mitochondrial disruption, and impaired microtubule function [73]. Hyperphosphorylated tau in particular is thought to lead to neurodegeneration and brain atrophy via disruption of its microtubule-stabilizing role, in addition to the influence of tau aggregates on functional protein trafficking, resulting in axonal and dendritic transport deficits [74]. Neurodegeneration in brain regions associated with cognitive function may thus help explain the cognitive decline observed in AD. However, our finding that ^{18}F-AV-1451 retention was associated with memory decline but not widespread brain volume loss suggests that atrophy in areas relevant for cognitive function may not be the only mechanism by which tau accumulation can influence cognition. Indeed, some have suggested that alterations in the integrity of functional brain networks mediated by AD pathology may anticipate cognitive changes in preclinical AD [75].

This study has several limitations. The relationships between PET tau and cognitive and volume declines were assessed retrospectively rather than prospectively due to the relatively recent implementation of tau PET in the BLSA. For this same reason, our sample size was limited, particularly for amyloid positive individuals. Future studies in a larger sample will be necessary to more fully investigate associations between amyloid, ^{18}F-AV-1451 retention, and time.

Our study also has several strengths. Our sample consisted of cognitively normal individuals from the BLSA, enabling us to study individuals in the early stages of tau pathology. In addition, by avoiding analyses of ^{18}F-AV-1451 signal in the hippocampus, we address the potential pitfall of choroid plexus signal contamination. Finally, our study takes advantage of the considerable amount of cognitive testing and volumetric data from the BLSA that allow us to make inferences about the influence of PET tau on retrospective longitudinal declines.

Overall, our results point to a relationship between tau pathology and early changes in cognition in older individuals, even for those without a high degree of pathology or cognitive impairment. These findings also suggest the importance of ^{18}F-AV-1451 PET for characterizing tau pathology in cognitively intact individuals and as a potential tool for predicting cognitive change early in AD progression. Future studies should investigate prospective cognitive and volumetric changes in relation to both timing and spread of tau deposition and their utility in predicting the trajectory of AD pathologies and symptoms. Further, effects of tau deposition on changes in functional connectivity in brain networks underlying cognitive function may provide additional insights into the relationship between pathology and cognitive decline in preclinical individuals.

5. Acknowledgments

We thank the Baltimore Longitudinal Study of Aging participants and staff; the Laboratory of Behavioral Neuroscience Neuropsychology Testing Group; Noble George, Daniel Holt, Hong Fan, and the rest of the Johns Hopkins PET facility staff for their dedication to the BLSA studies and their assistance, and the Center for Biomedical Image Computing and Analytics for providing MUSE labels and their contributions to MRI analysis. We received valuable feedback from our colleagues at the National Institute on Aging, in particular from Dr. Lori Beason-Held on neuroanatomy, for which we are grateful. We also thank Avid Radiopharmaceuticals for enabling the use of the ^{18}F-AV-1451 tracer and providing the precursor. Avid

Radiopharmaceuticals did not provide direct funding for any of the PET studes nor personnel and were not involved in data analysis or interpretation.

6. Funding

This research was supported by the Intramural Research Program of the National Institute on Aging, National Institutes of Health.

References

1. Goedert M, Spillantini MG, Jakes R, Rutherford D, Crowther RA. Multiple isoforms of human microtubule-associated protein tau: sequences and localization in neurofibrillary tangles of Alzheimer's disease. *Neuron* 1989;3(4):519–26. doi:10.1016/0896-6273(89)90210-9.

2. Nelson PT, Alafuzoff I, Bigio EH, Bouras C, Braak H, Cairns NJ, Castellani RJ, Crain BJ, Davies P, Del Tredici K, Duyckaerts C, Frosch MP, Haroutunian V, Hof PR, Hulette CM, Hyman BT, Iwatsubo T, Jellinger KA, Jicha GA, Kövari E, Kukull WA, Leverenz JB, Love S, Mackenzie IR, Mann DM, Masliah E, McKee AC, Montine TJ, Morris JC, Schneider JA, Sonnen JA, Thal DR, Trojanowski JQ, Troncoso JC, Wisniewski T, Woltjer RL, Beach TG. Correlation of Alzheimer disease neuropathologic changes with cognitive status: a review of the literature. *Journal of Neuropathology and Experimental Neurology* 2012;71(5):362–81. doi:10.1097/NEN.0b013e31825018f7.

3. Crary JF, Trojanowski JQ, Schneider JA, Abisambra JF, Abner EL, Alafuzoff I, Arnold SE, Attems J, Beach TG, Bigio EH, Cairns NJ, Dickson DW, Gearing M, Grinberg LT, Hof PR, Hyman BT, Jellinger K, Jicha GA, Kovacs GG, Knopman DS, Kofler J, Kukull WA, Mackenzie IR, Masliah E, McKee A, Montine TJ, Murray ME, Neltner JH, Santa-Maria I, Seeley WW, Serrano-Pozo A, Shelanski ML, Stein T, Takao M, Thal DR, Toledo JB, Troncoso JC, Vonsattel JP, White CL, Wisniewski T, Woltjer RL, Yamada M, Nelson PT. Primary age-related tauopathy (PART): a common pathology associated with human aging. *Acta Neuropathologica* 2014;128(6):755–66. doi:10.1007/s00401-014-1349-0.

4. Duyckaerts C, Braak H, Brion JP, Buée L, Del Tredici K, Goedert M, Halliday G, Neumann M, Spillantini MG, Tolnay M, Uchihara T. PART is part of Alzheimer disease. *Acta Neuropathologica* 2015;129(5):749–56. doi:10.1007/s00401-015-1390-7.

5. Bell WR, An Y, Kageyama Y, English C, Rudow GL, Pletnikova O, Thambisetty M, O'Brien R, Moghekar AR, Albert MS, Rabins PV, Resnick SM, Troncoso JC. Neuropathologic, genetic, and longitudinal cognitive profiles in primary age-related tauopathy (PART) and Alzheimer's disease. *Alzheimer's & Dementia* 2019;15(1):8–16. doi:10.1016/j.jalz.2018.07.215.

6. Sperling RA, Aisen PS, Beckett LA, Bennett DA, Craft S, Fagan AM, Iwatsubo T, Jack CR, Kaye J, Montine TJ, Park DC, Reiman EM, Rowe CC, Siemers E, Stern Y, Yaffe K, Carrillo MC, Thies B, Morrison-Bogorad M, Wagster MV, Phelps CH. Toward defining the preclinical stages of Alzheimer's disease: Recommendations from the National Institute on Aging-Alzheimer's Association workgroups on diagnostic guidelines for Alzheimer's disease. *Alzheimer's & Dementia* 2011;7(3):280–92. doi:10.1016/j.jalz.2011.03.003.

7. Jack CR, Knopman DS, Jagust WJ, Petersen RC, Weiner MW, Aisen PS, Shaw LM, Vemuri P, Wiste HJ, Weigand SD, Lesnick TG, Pankratz VS, Donohue MC, Trojanowski JQ. Tracking pathophysiological processes in Alzheimer's disease: an updated hypothetical model of dynamic biomarkers. *The Lancet Neurology* 2013;12(2):207–16. doi:10.1016/S1474-4422(12)70291-0.

8. Braak H, Braak E. Neuropathological stageing of Alzheimer-related changes. *Acta Neuropathologica* 1991;82(4):239–59. doi:10.1007/BF00308809.

9. Brier MR, Gordon B, Friedrichsen K, McCarthy J, Stern A, Christensen J, Owen C, Aldea P, Su Y, Hassenstab J, Cairns NJ, Holtzman DM, Fagan AM, Morris JC, Benzinger TLS, Ances BM. Tau and Aβ imaging, CSF measures, and cognition in Alzheimer's disease. *Science Translational Medicine* 2016;8(338):338ra66. doi:10.1126/scitranslmed.aaf2362.

10. Maass A, Landau S, Baker SL, Horng A, Lockhart SN, La Joie R, Rabinovici GD, Jagust WJ, Alzheimer's Disease Neuroimaging Initiative . Comparison of multiple tau-PET measures as biomarkers in aging and Alzheimer's disease. *NeuroImage* 2017;157:448–63. doi:10.1016/j.neuroimage.2017.05.058.

11. Wang L, Benzinger TL, Su Y, Christensen J, Friedrichsen K, Aldea P, McConathy J, Cairns NJ, Fagan AM, Morris JC, Ances BM. Evaluation of tau imaging in staging Alzheimer disease and revealing interactions between β-amyloid and tauopathy. *JAMA Neurology* 2016;73(9):1070–7. doi:10.1001/jamaneurol.2016.2078.

12. Pontecorvo MJ, Devous MD, Navitsky M, Lu M, Salloway S, Schaerf FW, Jennings D, Arora AK, McGeehan A, Lim NC, Xiong H, Joshi AD, Siderowf A, Mintun MA, investigators FAA. Relationships between flortaucipir PET tau binding and amyloid burden, clinical diagnosis, age and cognition. *Brain* 2017;140(3):748–63. doi:10.1093/brain/aww334.

13. Das SR, Xie L, Wisse LEM, Ittyerah R, Tustison NJ, Dickerson BC, Yushkevich PA, Wolk DA, Alzheimer's Disease Neuroimaging Initiative . Longitudinal and cross-sectional structural magnetic resonance imaging correlates of AV-1451 uptake. *Neurobiology of Aging* 2018;66:49–58. doi:10.1016/j.neurobiolaging.2018.01.024.

14. Iaccarino L, Tammewar G, Ayakta N, Baker SL, Bejanin A, Boxer AL, Gorno-Tempini ML, Janabi M, Kramer JH, Lazaris A, Lockhart SN, Miller BL, Miller ZA, O'Neil JP, Ossenkoppele R, Rosen HJ, Schonhaut DR, Jagust WJ, Rabinovici GD. Local and distant relationships between amyloid, tau and neurodegeneration in Alzheimer's disease. *NeuroImage: Clinical* 2018;17:452–64. doi:10.1016/j.nicl.2017.09.016.

15. Aschenbrenner AJ, Gordon BA, Benzinger TLS, Morris JC, Hassenstab JJ. Influence of tau PET, amyloid PET, and hippocampal volume on cognition in Alzheimer disease. *Neurology* 2018;91(9):e859–66. doi:10.1212/WNL.0000000000006075.

16. Koychev I, Gunn RN, Firouzian A, Lawson J, Zamboni G, Ridha B, Sahakian BJ, Rowe JB, Thomas A, Rochester L, Ffytche D, Howard R, Zetterberg H, MacKay C, Lovestone S, Deep and Frequent Phenotyping study team . PET tau and amyloid-β burden in mild Alzheimer's disease: divergent relationship with age, cognition, and cerebrospinal fluid biomarkers. *Journal of Alzheimer's Disease* 2017;60(1):283–93. doi:10.3233/JAD-170129.

17. Pontecorvo MJ, Devous MD, Kennedy I, Navitsky M, Lu M, Galante N, Salloway S, Doraiswamy PM, Southekal S, Arora AK, McGeehan A, Lim NC, Xiong H, Truocchio SP, Joshi AD, Shcherbinin S, Teske B, Fleisher AS, Mintun MA. A multicentre longitudinal study of flortaucipir (^{18}F) in normal ageing, mild cognitive impairment and Alzheimer's disease dementia. *Brain* 2019;:1–13doi:10.1093/brain/awz090.

18. Schöll M, Lockhart SN, Schonhaut DR, O'Neil JP, Janabi M, Ossenkoppele R, Baker SL, Vogel JW, Faria J, Schwimmer HD, Rabinovici GD, Jagust WJ. PET imaging of tau deposition in the aging human brain. *Neuron* 2016;89(5):971–82. doi:10.1016/j.neuron.2016.01.028.

19. Buckley RF, Hanseeuw B, Schultz AP, Vannini P, Aghjayan SL, Properzi MJ, Jackson JD, Mormino EC, Rentz DM, Sperling RA, Johnson KA, Amariglio RE. Region-specific association of subjective cognitive decline with tauopathy independent of global β-amyloid burden. *JAMA Neurology* 2017;74(12):1455–63. doi:10.1001/jamaneurol.2017.2216.

20. Schultz SA, Gordon BA, Mishra S, Su Y, Perrin RJ, Cairns NJ, Morris JC, Ances BM, Benzinger TLS. Widespread distribution of tauopathy in preclinical Alzheimer's disease. *Neurobiology of Aging* 2018;72:177–85. doi:10.1016/j.neurobiolaging.2018.08.022.

21. Sepulcre J, Schultz AP, Sabuncu M, Gomez-Isla T, Chhatwal J, Becker A, Sperling R, Johnson KA. In vivo tau, amyloid, and gray matter profiles in the aging brain. *Journal of Neuroscience* 2016;36(28):7364–74. doi:10.1523/JNEUROSCI.0639-16.2016.

22. Saint-Aubert L, Lemoine L, Chiotis K, Leuzy A, Rodriguez-Vieitez E, Nordberg A. Tau PET imaging: present and future directions. *Molecular Neurodegeneration* 2017;12(19):1–21. doi:10.1186/s13024-017-0162-3.

23. Baker SL, Harrison TM, Maaß A, La Joie R, Jagust W. Effect of off-target binding on ^{18}F-Flortaucipir variability in healthy controls across the lifespan. *Journal of Nuclear Medicine* 2019;:jnumed.118.224113doi:10.2967/jnumed.118.224113.

24. Morris JC. The Clinical Dementia Rating (CDR): Current version and scoring rules. 1993.

25. Fuld PA. Psychological testing in the differential diagnosis of the dementias. In: Katzman R, Terry RD, Bick KL, eds. *Alzheimer's disease: Senile dementia and related disorders*. New York, NY: Raven Press; 1978:185–93.

26. Doshi J, Erus G, Ou Y, Resnick SM, Gur RC, Gur RE, Satterthwaite TD, Furth S, Davatzikos C. MUSE: MUlti-atlas region Segmentation utilizing Ensembles of registration algorithms and parameters, and locally optimal atlas selection. *NeuroImage* 2016;127(2016):186–95. doi:10.1016/j.neuroimage.2015.11.073.

27. Jack CR, Twomey K, Zinsmeister AR, Sharbrough FW, Petersen C, Cascino GD. Anterior temporal lobes and hippocampal formations: normative volumetric measurements from MR images in young adults. *Radiology* 1989;172:549–54.

28. Ashburner J, Friston KJ. Spatial transformation of images. In: Frackowiak RSJ, Friston KJ, Frith C, Dolan R, Mazziotta JC, eds. *Human Brain Function*. Academic Press USA; 1997:43–58.

29. Jenkinson M, Bannister P, Brady M, Smith S. Improved optimization for the robust and accurate linear registration and motion correction of brain images. *NeuroImage* 2002;17(2):825–41. doi:10.1006/nimg.2002.1132.

30. Jenkinson M, Beckmann CF, Behrens TE, Woolrich MW, Smith SM. FSL. *NeuroImage* 2012;62(2):782–90. doi:10.1016/j.neuroimage.2011.09.015.

31. Zhou Y, Resnick SM, Ye W, Fan H, Holt DP, Klunk WE, Mathis CA, Dannals R, Wong DF. Using a reference tissue model with spatial constraint to quantify [^{11}C]Pittsburgh compound B PET for early diagnosis of Alzheimer's disease. *NeuroImage* 2007;36(2):298–312. doi:10.1016/j.neuroimage.2007.03.004.

32. Thomas BA, Erlandsson K, Modat M, Thurfjell L, Vandenberghe R, Ourselin S, Hutton BF. The importance of appropriate partial volume correction for PET quantification in Alzheimer's disease. *European Journal of Nuclear Medicine and Molecular Imaging* 2011;38(6):1104–19. doi:10.1007/s00259-011-1745-9.

33. Thomas BA, Cuplov V, Bousse A, Mendes A, Thielemans K, Hutton BF, Erlandsson K. PETPVC: a toolbox for performing partial volume correction techniques in positron emission tomography. *Physics in Medicine and Biology* 2016;61(22):7975–93. doi:10.1088/0031-9155/61/22/7975.

34. Baker SL, Maass A, Jagust WJ. Considerations and code for partial volume correcting [^{18}F]-AV-1451 tau PET data. *Data in Brief* 2017;15:648–57. doi:10.1016/j.dib.2017.10.024.

35. Diedrichsen J, Balsters JH, Flavell J, Cussans E, Ramnani N. A probabilistic MR atlas of the human cerebellum. *NeuroImage* 2009;46(1):39–46. doi:10.1016/j.neuroimage.2009.01.045.

36. Avants BB, Tustison NJ, Song G, Cook Pa, Klein A, Gee JC. A reproducible evaluation of ANTs similarity metric performance in brain image registration. *NeuroImage* 2011;54(3):2033–44. doi:10.1016/j.neuroimage.2010.09.025.

37. Gorgolewski K, Burns CD, Madison C, Clark D, Halchenko YO, Waskom ML, Ghosh SS. Nipype: a flexible, lightweight and extensible neuroimaging data processing framework in python. *Frontiers in Neuroinformatics* 2011;5(13):1–15. doi:10.3389/fninf.2011.00013.

38. Delis DC, Kramer JH, Kaplan E, Ober BA. The California Verbal Learning Test. San Antonio, TX: Psychological Corporation; 1987.

39. Reitan RM. Trail making test: Manual for administration and scoring. Tucson, AZ: Reitan Neuropsychological Laboratory; 1992.

40. Wechsler D. Wechsler adult intelligence scale-revised. Revised ed.; San Antonio, TX: Psychological Corporation; 1981.

41. Newcombe F. Missile wounds of the brain: a study of psychological deficits. Oxford: Oxford University Press; 1969.

42. Benton AL. Differential behavioral effects in frontal lobe disease. *Neuropsychologia* 1968;6(1):53–60. doi:10.1016/0028-3932(68)90038-9.

43. Wilson JR, De Fries JC, Mc Clearn GE, Vandenberg SG, Johnson RC, Rashad MN. Cognitive abilities: Use of family data as a control to assess sex and age differences in two ethnic groups. *International Journal of Aging and Human Development* 1975;6(3):261–76. doi:10.2190/BBJP-XKUG-C6EW-KYB7.

44. Rouleau I, Salmon DP, Butters N, Kennedy C, McGuire K. Quantitative and qualitative analyses of clock drawings in Alzheimer's and Huntington's disease. *Brain and Cognition* 1992;18(1):70–87. doi:10.1016/0278-2626(92)90112-Y.

45. Allen EA, Erhardt EB, Calhoun VD. Data visualization in the neurosciences: overcoming the curse of dimensionality. *Neuron* 2012;74(4):603–8. doi:10.1016/j.neuron.2012.05.001.

46. Notter M, Gale D, Herholz P, Markello R, Notter-Bielser ML, Whitaker K. AtlasReader: A Python package to generate coordinate tables, region labels, and informative figures from statistical MRI images. *Journal of Open Source Software* 2019;4(34):1257. doi:10.21105/joss.01257.

47. Talairach J, Tournoux P. Co-planar stereotaxic atlas of the human brain. New York, NY: Thieme; 1988.

48. Lacadie CM, Fulbright RK, Rajeevan N, Constable RT, Papademetris X. More accurate Talairach coordinates for neuroimaging using non-linear registration. *NeuroImage* 2008;42(2):717–25. doi:10.1016/j.neuroimage.2008.04.240.

49. Tosun D, Landau S, Aisen PS, Petersen RC, Mintun M, Jagust W, Weiner MW, Alzheimer's Disease Neuroimaging Initiative . Association between tau deposition and antecedent amyloid-β accumulation rates in normal and early symptomatic individuals. *Brain* 2017;140(5):1499–512. doi:10.1093/brain/awx046.

50. Abraham A, Pedregosa F, Eickenberg M, Gervais P, Mueller A, Kossaifi J, Gramfort A, Thirion B, Varoquaux G. Machine learning for neuroimaging with scikit-learn. *Frontiers in Neuroinformatics* 2014;8(14):1–10. doi:10.3389/fninf.2014.00014. arXiv:1412.3919.

51. Pinheiro JC, Bates DM, DebRoy S, Sarkar D, R Core Team . nlme: Linear and nonlinear mixed effects models. 2015. URL: http://cran.r-project.org/package=nlme.

52. Kurtzer GM, Sochat V, Bauer MW. Singularity: scientific containers for mobility of compute. *PloS ONE* 2017;12(5):e0177459. doi:10.1371/journal.pone.0177459.

53. Xie Y. Dynamic documents with R and knitr. 2nd ed.; Chapman and Hall/CRC; 2015. ISBN 978-1498716963.

54. Xie Y. knitr: A general-purpose package for dynamic report generation in R. 2018.

55. Zhu H. kableExtra: Construct complex table with 'kable' and pipe syntax. 2019.

56. Hlavac M. stargazer: Well-formatted regression and summary statistics tables. 2018. URL: https://cran.r-project.org/package=stargazer.

57. Wickham H. ggplot2: Elegant Graphics for Data Analysis. Springer-Verlag New York; 2016. ISBN 978-3-319-24277-4.

58. Kassambara A. ggpubr: 'ggplot2' based publication ready plots. 2018. URL: `https://cran.r-project.org/package=ggpubr`.

59. Maumet C, Auer T, Bowring A, Chen G, Das S, Flandin G, Ghosh S, Glatard T, Gorgolewski KJ, Helmer KG, Jenkinson M, Keator DB, Nichols BN, Poline JB, Reynolds R, Sochat V, Turner J, Nichols TE. Sharing brain mapping statistical results with the neuroimaging data model. *Scientific Data* 2016;3(160102):1–15. doi:10.1038/sdata.2016.102.

60. Gorgolewski KJ, Varoquaux G, Rivera G, Schwarz Y, Ghosh SS, Maumet C, Sochat VV, Nichols TE, Poldrack RA, Poline JB, Yarkoni T, Margulies DS. NeuroVault.org: a web-based repository for collecting and sharing unthresholded statistical maps of the human brain. *Frontiers in Neuroinformatics* 2015;9(8):1–9. doi:10.3389/fninf.2015.00008.

61. Marquié M, Normandin MD, Vanderburg CR, Costantino IM, Bien EA, Rycyna LG, Klunk WE, Mathis CA, Ikonomovic MD, Debnath ML, Vasdev N, Dickerson BC, Gomperts SN, Growdon JH, Johnson KA, Frosch MP, Hyman BT, Gómez-Isla T. Validating novel tau positron emission tomography tracer [F-18]-AV-1451 (T807) on postmortem brain tissue. *Annals of Neurology* 2015;78(5):787–800. doi:10.1002/ana.24517. arXiv:15334406.

62. Ottoy J, Verhaeghe J, Niemantsverdriet E, Engelborghs S, Stroobants S, Staelens S. A simulation study on the impact of the blood flow-dependent component in [^{18}F]AV45 SUVR in Alzheimer's disease. *PloS ONE* 2017;12(12):e0189155. doi:10.1371/journal.pone.0189155.

63. Stancu IC, Vasconcelos B, Terwel D, Dewachter I. Models of β-amyloid induced tau-pathology: the long and "folded" road to understand the mechanism. *Molecular Neurodegeneration* 2014;9(51):1–14. doi:10.1186/1750-1326-9-51.

64. Jack CR, Wiste HJ, Schwarz CG, Lowe VJ, Senjem ML, Vemuri P, Weigand SD, Therneau TM, Knopman DS, Gunter JL, Jones DT, Graff-Radford J, Kantarci K, Roberts RO, Mielke MM, Machulda MM, Petersen RC. Longitudinal tau PET in ageing and Alzheimer's disease. *Brain* 2018;141(5):1517–28. doi:10.1093/brain/awy059.

65. Harrison TM, La Joie R, Maass A, Baker SL, Swinnerton K, Fenton L, Mellinger TJ, Edwards L, Pham J, Miller BL, Rabinovici GD, Jagust WJ. Longitudinal tau accumulation and atrophy in aging and Alzheimer disease. *Annals of Neurology* 2019;85(2):229–40. doi:10.1002/ana.25406.

66. Buckley RF, Mormino EC, Rabin JS, Hohman TJ, Landau S, Hanseeuw BJ, Jacobs HIL, Papp KV, Amariglio RE, Properzi MJ, Schultz AP, Kirn D, Scott MR, Hedden T, Farrell M, Price J, Chhatwal J, Rentz DM, Villemagne VL, Johnson KA, Sperling RA. Sex differences in the association of global amyloid and regional tau deposition measured by positron emission tomography in clinically normal older adults. *JAMA Neurology* 2019;doi:10.1001/jamaneurol.2018.4693.

67. Barnes LL, Wilson RS, Bienias JL, Schneider JA, Evans DA, Bennett DA. Sex differences in the clinical manifestations of Alzheimer disease pathology. *Archives of General Psychiatry* 2005;62(6):685–91.

68. Howell JC, Watts KD, Parker MW, Wu J, Kollhoff A, Wingo TS, Dorbin CD, Qiu D, Hu WT. Race modifies the relationship between cognition and Alzheimer's disease cerebrospinal fluid biomarkers. *Alzheimer's Research & Therapy* 2017;9(88):1–10. doi:10.1186/s13195-017-0315-1.

69. Graff-Radford NR, Besser LM, Crook JE, Kukull WA, Dickson DW. Neuropathologic differences by race from the National Alzheimer's Coordinating Center. *Alzheimer's & Dementia* 2016;12(6):669–77. doi:10.1016/j.jalz.2016.03.004.

70. Lee CM, Jacobs HIL, Marquié M, Becker JA, Andrea NV, Jin DS, Schultz AP, Frosch MP, Gómez-Isla T, Sperling RA, Johnson KA. ^{18}F-Flortaucipir binding in choroid plexus: related to race and hippocampus signal. *Journal of Alzheimer's Disease* 2018;62(4):1691–702. doi:10.3233/JAD-170840.

71. Bilgel M, An Y, Helphrey J, Elkins W, Gomez G, Wong DF, Davatzikos C, Ferrucci L, Resnick SM. Effects of amyloid pathology and neurodegeneration on cognitive change in cognitively normal adults. *Brain* 2018;8(August):2475–85. doi:10.1093/brain/awy150.

72. Ossenkoppele R, Schonhaut DR, Schöll M, Lockhart SN, Ayakta N, Baker SL, O'Neil JP, Janabi M, Lazaris A, Cantwell A, Vogel J, Santos M, Miller ZA, Bettcher BM, Vossel KA, Kramer JH, Gorno-Tempini ML, Miller BL, Jagust WJ, Rabinovici GD. Tau PET patterns mirror clinical and neuroanatomical variability in Alzheimer's disease. *Brain* 2016;139(5):1551–67. doi:10.1093/brain/aww027.

73. Spires-Jones TL, Hyman BT. The intersection of amyloid beta and tau at synapses in Alzheimer's disease. *Neuron* 2014;82(4):756–71. doi:10.1016/j.neuron.2014.05.004.

74. Wang JZ, Xia YY, Grundke-Iqbal I, Iqbal K. Abnormal hyperphosphorylation of tau: sites, regulation, and molecular mechanism of neurofibrillary degeneration. *Journal of Alzheimer's Disease* 2013;33:S123–39. doi:10.3233/JAD-2012-129031.

75. Buckley RF, Schultz AP, Hedden T, Papp KV, Hanseeuw BJ, Marshall G, Sepulcre J, Smith EE, Rentz DM, Johnson KA, Sperling RA, Chhatwal JP. Functional network integrity presages cognitive decline in preclinical Alzheimer disease. *Neurology* 2017;89(1):29–37. doi:10.1212/WNL.0000000000004059.

Appendix A. Determination of amyloid status

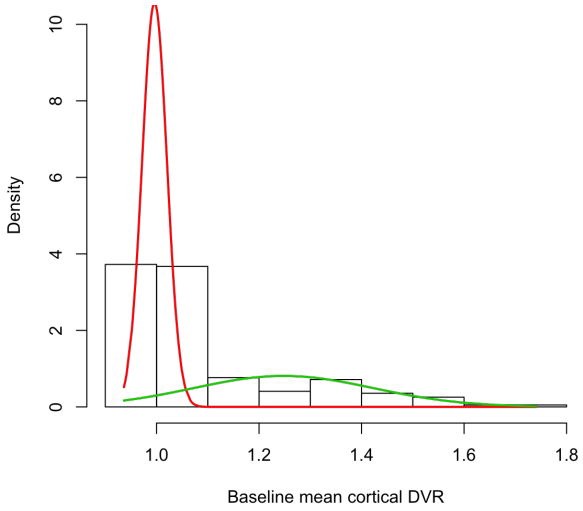

Figure A.1: Result of the two-class Gaussian mixture model fitted on baseline mean cortical DVR. Red and green density curves correspond to the amyloid– and amyloid+ groups, respectively. Mean cortical DVR corresponding to the intersection of the two densities is the threshold for determining amyloid−/+ status.

Appendix B. Partial volume correction of ^{18}F-AV-1451 PET

The MUSE ROIs used for the geometric matrix transfer step of RBV partial volume correction method were: background, ventricles and cerebrospinal fluid, basal ganglia, thalamus, brainstem, hippocampus, amygdala, cerebral white matter, inferior frontal gray matter, lateral frontal gray matter, medial frontal gray matter, opercular frontal gray matter, lateral parietal gray matter, medial parietal gray matter, fusiform, lateral temporal gray matter, supratemporal gray matter, inferior occipital gray matter, lateral occipital gray matter, medial occipital gray matter, limbic medial temporal gray matter, cingulate gray matter, insula gray matter, cerebellar white matter, cerebellar gray matter, cerebellar vermis).

Appendix C. Regional analyses of predictors of ^{18}F-AV-1451 SUVR

To corroborate the observed voxel-wise effects of predictors of ^{18}F-AV-1451 SUVR, we used linear regression to test the relationship between demographics, amyloid positivity, and regional ^{18}F-AV-1451 SUVR. ROIs within areas indicated by the voxel-wise analyses were selected to be tested for each predictor in the model. In agreement with voxel-wise results, amyloid status modulated the association of greater age with ^{18}F-AV-1451 SUVR in the medial occipital gray matter ($\beta = 0.009, \text{SE} = 0.003, p = 0.003$). A main effect of age in amyloid positive individuals was also associated with greater ^{18}F-AV-1451 SUVR in the bilateral putamen ($\beta = 0.024, \text{SE} = 0.008, p = 0.005$) and a main effect of age in amyloid negative individuals was associated with lower ^{18}F-AV-1451 retention in the ventricles and cerebrospinal fluid ($\beta = -0.007, \text{SE} = 0.002, p = 0.002$). Amyloid positive individuals also exhibited greater ^{18}F-AV-1451 SUVR in the bilateral inferior temporal gyrus compared to amyloid negative individuals ($\beta = 0.095, \text{SE} = 0.028, p = 0.002$). In addition, male sex was associated with greater ^{18}F-AV-1451 SUVR in the frontal gray matter ($\beta = 0.102, \text{SE} = 0.024, p < 0.001$). Finally, black individuals showed greater ^{18}F-AV-1451 retention in the superior frontal gyrus ($\beta = 0.137, \text{SE} = 0.032, p < 0.001$) (Table C.1).

Table C.1: Associations between participant demographics, amyloid status, and regional ^{18}F-AV-1451 SUVR. Estimated fixed effects are reported along with their standard errors in parentheses.

	Dependent variable: Regional ^{18}F-AV-1451 SUVR					
	Medial occipital GM	Putamen	Ventricles and CSF	Inferior temporal gyrus	Frontal gray matter	Superior frontal gyrus
Intercept	1.139*** (0.011) p = 0.000	1.632*** (0.027) p = 0.000	0.924*** (0.019) p = 0.000	1.243*** (0.012) p = 0.000	1.199*** (0.011) p = 0.000	1.165*** (0.013) p = 0.000
Age at PET scan	−0.002 (0.001) p = 0.148	0.010** (0.003) p = 0.004	−0.007** (0.002) p = 0.002	0.00002 (0.001) p = 0.987	−0.001 (0.001) p = 0.530	0.001 (0.002) p = 0.531
Sex (ref = female)	0.046* (0.022) p = 0.046	0.153** (0.057) p = 0.010	−0.015 (0.040) p = 0.707	0.049* (0.024) p = 0.050	0.102*** (0.024) p = 0.0001	0.099*** (0.028) p = 0.001
Race (ref = non-black)	0.102*** (0.026) p = 0.0004	0.069 (0.067) p = 0.306	0.056 (0.047) p = 0.239	0.065* (0.029) p = 0.029	0.092** (0.028) p = 0.003	0.137*** (0.032) p = 0.0002
Amyloid group (ref = amyloid–)	0.040 (0.026) p = 0.127	0.086 (0.066) p = 0.197	0.055 (0.046) p = 0.240	0.095** (0.028) p = 0.002	0.072* (0.028) p = 0.012	0.078* (0.032) p = 0.019
Age × amyloid group	0.009** (0.003) p = 0.003	0.015 (0.007) p = 0.053	−0.002 (0.005) p = 0.708	0.005 (0.003) p = 0.118	0.010** (0.003) p = 0.003	0.009* (0.004) p = 0.014
Note:						*p<0.05; **p<0.01; ***p<0.001

Appendix D. Peak tables

For each peak and subpeak, the label with the greatest number of hits within a 9 mm-wide cube range search as determined using the Talairach Client is displayed in the tables below. For top hits that were not assigned a Brodmann area (BA) in the Talairach client output, if there was another hit with the same anatomical label as the top hit, we report their BA where applicable. All label and BA assignments were confirmed via visual inspection. (Sub)Peaks are sorted by the laterality (Bilateral, Left hemisphere, or Right hemisphere) of the cluster they belong to, then the brain region (Frontal, Parietal, Temporal, Occipital, Limbic, Midbrain, Pons, Subcortical, Cerebellum, or a combination thereof) the cluster falls into. We omitted subpeaks with repeated labels within a cluster, and display only the one with the largest T-value. BA = Brodmann area, L = Left, R = Right.

Table D.1: Cluster peaks and subpeaks for the age × amyloid status interaction.

Label	Volume (mm^3)	MNI (x, y, z)	T-value
Bilateral			
Cingulate			
L Cingulate Gyrus BA 31	783	(-9, -52, 25)	4.56
R Cingulate Gyrus BA 31		(2, -47, 29)	3.83
Left hemisphere			
Frontal			
Middle Frontal Gyrus BA 10	604	(-34, 50, 8)	4.20
Middle Frontal Gyrus BA 6	993	(-42, 4, 46)	5.09
Precentral Gyrus BA 6		(-40, -1, 32)	4.38
Frontal, Cingulate			
Superior Frontal Gyrus BA 9	928	(-15, 37, 42)	4.29
Anterior Cingulate BA 32		(-15, 35, 17)	4.24
Frontal, Parietal			
Insula BA 13	1588	(-39, -10, 18)	3.88
Postcentral Gyrus BA 43		(-52, -15, 19)	4.56
Frontal, Temporal			
Frontal Sub-Gyral	845	(-47, 10, 11)	4.63
Superior Temporal Gyrus BA 22		(-51, 5, -1)	4.78
Occipital			
Cuneus BA 18	670	(0, -87, 18)	5.13
	640	(-5, -97, 1)	4.89
Right hemisphere			
Cingulate			
Anterior Cingulate BA 32	409	(7, 43, 6)	5.06
Frontal			
Frontal Sub-Gyral	1320	(24, 41, -6)	4.87
Inferior Frontal Gyrus BA 47		(34, 32, -9)	5.75
Superior Frontal Gyrus BA 6/8	614	(12, 25, 56)	4.66
Occipital			
Cuneus BA 17	560	(15, -92, 7)	4.58
Middle Occipital Gyrus BA 18		(20, -94, 18)	4.00
Parietal			
Inferior Parietal Lobule BA 40	793	(57, -36, 25)	4.41
Postcentral Gyrus BA 2		(54, -25, 32)	3.97
Temporal			
Middle Temporal Gyrus BA 37	485	(56, -47, -16)	4.58
Temporal, Occipital			
Middle Temporal Gyrus BA 39	1326	(44, -72, 14)	4.23
Middle Occipital Gyrus BA 19		(45, -77, -8)	5.21

Table D.2: Cluster peaks and subpeaks for the main effect of age among amyloid+ individuals.

Label	Volume (mm^3)	MNI (x, y, z)	T-value
Left hemisphere			
Subcortical			
Putamen	515	(-20, 8, 3)	4.30
Right hemisphere			
Frontal			
Inferior Frontal Gyrus BA 47	415	(35, 31, -9)	5.47
Occipital			
Middle Occipital Gyrus BA 19	557	(45, -77, -8)	5.75
Subcortical			
Putamen	2660	(31, 4, 1)	5.38

Table D.3: Cluster peaks and subpeaks for the main effect of age among amyloid– individuals.

Label	Volume (mm^3)	MNI (x, y, z)	T-value
Bilateral			
Frontal, Parietal, Temporal, Cingulate, Midbrain, Pons, Subcortical			
L Frontal Sub-Gyral	63393	(-21, -29, 25)	-5.00
L Inferior Frontal Gyrus BA 47		(-30, 21, -15)	-4.48
L Medial Frontal Gyrus BA 10		(-2, 62, 18)	-5.20
L Medial Frontal Gyrus BA 8		(-2, 30, 46)	-4.83
L Medial Frontal Gyrus BA 9		(0, 46, 35)	-6.36
L Precentral Gyrus		(-51, -11, 26)	-4.69
L Precentral Gyrus BA 4		(-57, -13, 38)	-3.98
L Precentral Gyrus BA 43		(-57, -9, 8)	-4.48
L Precentral Gyrus BA 6		(-41, -15, 34)	-4.77
L Subcallosal Gyrus BA 25		(0, 14, -16)	-5.17
L Parietal Sub-Gyral		(-23, -53, 32)	-4.41
L Postcentral Gyrus BA 40		(-58, -19, 15)	-4.76
L Superior Temporal Gyrus BA 22		(-52, 5, -2)	-5.68
L Temporal Sub-Gyral		(-24, -56, 14)	-5.90
L Anterior Cingulate BA 24		(0, 33, 12)	-5.06
L Cingulate Gyrus BA 23		(0, -26, 26)	-4.13
L Cingulate Gyrus BA 32		(-14, 15, 27)	-5.44
L Posterior Cingulate BA 30		(-14, -56, 4)	-4.28
R Anterior Cingulate BA 24		(7, 38, 0)	-4.35
R Cingulate Gyrus BA 32		(2, 20, 31)	-4.47
L Midbrain		(-15, -28, -8)	-4.78
R Midbrain		(15, -26, -13)	-4.50
R Pons		(8, -23, -33)	-5.21
L Corpus Callosum		(-11, 29, 3)	-5.69
L Extra-Nuclear		(0, 0, -10)	-4.95
L Insula BA 13		(-42, -8, 11)	-5.48
L Lateral Ventricle		(-6, 2, 18)	-4.45
R Corpus Callosum		(1, 21, 16)	-5.10
R Extra-Nuclear		(9, 1, 4)	-3.95
R Thalamus Medial Dorsal Nucleus		(3, -18, 9)	-4.24
L Third Ventricle		(-1, -14, -2)	-5.13
Occipital, Cingulate			
L Cuneus BA 18	19742	(-4, -98, 10)	-5.09
L Cuneus BA 19		(-14, -96, 22)	-5.72
L Middle Occipital Gyrus BA 18		(-31, -95, 7)	-4.54
L Middle Occipital Gyrus BA 19		(-41, -88, 2)	-4.01
L Precuneus BA 31		(-5, -68, 30)	-4.21
R Cuneus BA 17		(15, -92, 7)	-5.06
R Cuneus BA 18		(4, -92, 18)	-4.98
R Cuneus BA 19		(14, -89, 37)	-4.46
R Cuneus BA 7		(16, -78, 30)	-5.06
R Middle Occipital Gyrus BA 18		(18, -96, 18)	-6.37
L Posterior Cingulate BA 23		(-1, -61, 11)	-4.54
R Posterior Cingulate BA 31		(12, -60, 18)	-5.94
L Inter-Hemispheric Fissure		(-4, -63, -3)	-4.18
Left hemisphere			

Cerebellum				
	Uvula	775	(0, -68, -37)	-5.45
Cingulate				
	Cingulate Gyrus BA 24	425	(-2, 4, 45)	-3.96
Frontal				
	Frontal Sub-Gyral	1476	(-28, 51, -2)	-4.37
	Middle Frontal Gyrus BA 10		(-31, 61, 11)	-4.16
	Middle Frontal Gyrus BA 11		(-33, 42, -9)	-3.73
	Superior Frontal Gyrus BA 10		(-20, 57, 6)	-3.81
Parietal				
	Inferior Parietal Lobule BA 40	806	(-57, -35, 23)	-4.46
Right hemisphere				
Frontal				
	Frontal Sub-Gyral	1735	(24, 40, -6)	-5.03
	Frontal Sub-Gyral Corpus Callosum		(22, 37, 10)	-3.94
	Frontal Sub-Gyral	458	(47, -2, 21)	-4.17
	Inferior Frontal Gyrus BA 44	402	(59, 17, 19)	-4.09
Frontal, Parietal				
	Precentral Gyrus BA 4	1696	(39, -19, 53)	-5.33
	Postcentral Gyrus BA 2		(46, -31, 54)	-3.98
Frontal, Parietal, Temporal, Subcortical				
	Frontal Sub-Gyral	2728	(23, -38, 31)	-4.16
	Parietal Sub-Gyral		(28, -49, 26)	-4.43
	Parahippocampal Gyrus BA 30		(22, -45, -1)	-3.78
	Extra-Nuclear		(25, -46, 14)	-4.72
Parietal, Temporal, Subcortical, Frontal-Temporal Space				
	Postcentral Gyrus BA 43	8051	(64, -11, 12)	-4.79
	Superior Temporal Gyrus BA 42		(65, -31, 18)	-4.77
	Temporal Sub-Gyral BA 41		(36, -36, 10)	-3.89
	Frontal-Temporal Space		(46, 1, -5)	-5.71
Subcortical				
	Corpus Callosum	768	(6, -43, 10)	-4.76
	Extra-Nuclear	691	(21, -14, 11)	-5.04
Temporal				
	Superior Temporal Gyrus BA 22	543	(69, -36, 6)	-4.58
Temporal, Occipital				
	Middle Temporal Gyrus BA 39	752	(56, -65, 14)	-4.40
	Middle Occipital Gyrus BA 19		(50, -81, 4)	-4.08

Table D.4: Cluster peaks and subpeaks for the main effect of amyloid status. Positive T-values indicate that ^{18}F-AV-1451 SUVR is greater among amyloid+ compared to amyloid– individuals.

Label	Volume (mm^3)	MNI (x, y, z)	T-value
Left hemisphere			
Occipital			
Cuneus BA 19	2486	(-15, -97, 21)	4.02
Middle Occipital Gyrus BA 18		(-28, -96, -5)	4.42
Middle Occipital Gyrus BA 19		(-32, -93, 11)	5.02
Superior Occipital Gyrus BA 19		(-36, -85, 28)	4.15
Temporal			
Middle Temporal Gyrus BA 21	579	(-63, -53, 5)	6.18
Right hemisphere			
Frontal			
Middle Frontal Gyrus BA 6	786	(32, 3, 52)	5.00
Occipital			
Cuneus BA 19	767	(13, -91, 31)	3.84
Middle Occipital Gyrus BA 18		(19, -95, 17)	4.93
Temporal			
Fusiform Gyrus	881	(39, -51, -13)	5.14
Middle Temporal Gyrus BA 37	471	(56, -60, 1)	5.60
Superior Temporal Gyrus BA 38	491	(51, 13, -30)	4.76
Temporal, Occipital			
Middle Temporal Gyrus BA 19	1434	(52, -76, 11)	4.45
Middle Occipital Gyrus BA 19		(44, -77, -8)	4.40

Table D.5: Cluster peaks and subpeaks for the main effect of sex. Positive T-values indicate that ^{18}F-AV-1451 SUVR is greater among men compared to women.

Label	Volume (mm^3)	MNI (x, y, z)	T-value
Bilateral			
Frontal, Cingulate, Subcortical			
L Medial Frontal Gyrus BA 11	30918	(-4, 57, -11)	4.18
R Frontal Sub-Gyral		(31, 22, 16)	4.26
R Inferior Frontal Gyrus BA 11		(19, 30, -16)	6.07
R Inferior Frontal Gyrus BA 46		(48, 30, 8)	5.61
R Inferior Frontal Gyrus BA 47		(30, 32, -10)	5.44
R Insula BA 13		(42, 11, -4)	6.04
R Medial Frontal Gyrus BA 10		(10, 53, -6)	4.79
R Medial Frontal Gyrus BA 9		(10, 42, 31)	3.89
R Middle Frontal Gyrus BA 10		(38, 48, 4)	4.57
R Middle Frontal Gyrus BA 11		(33, 51, -10)	4.40
R Rectal Gyrus BA 11		(7, 48, -22)	6.04
R Superior Frontal Gyrus BA 10		(24, 51, -2)	5.67
L Rectal Gyrus BA 11		(-6, 52, -22)	4.87
L Anterior Cingulate BA 32		(0, 47, -1)	3.84
R Anterior Cingulate BA 32		(13, 42, 4)	6.15
Frontal, Parietal, Cingulate			
L Frontal Sub-Gyral BA 6	41944	(-17, -9, 57)	4.39
L Medial Frontal Gyrus BA 6		(-4, 1, 63)	5.23
L Paracentral Lobule BA 5		(-10, -36, 59)	4.63
L Precentral Gyrus BA 4		(-21, -28, 73)	4.71
L Precentral Gyrus BA 6		(-28, -14, 56)	4.64
R Frontal Sub-Gyral		(20, 3, 50)	5.05
R Frontal Sub-Gyral BA 6		(20, -8, 55)	4.68
R Medial Frontal Gyrus BA 6		(5, -17, 60)	4.22
R Middle Frontal Gyrus BA 6		(34, -8, 63)	4.25
R Paracentral Lobule BA 6		(4, -32, 67)	4.80
R Precentral Gyrus BA 4		(28, -29, 64)	5.51
R Precentral Gyrus BA 6		(23, -20, 71)	5.27
R Superior Frontal Gyrus BA 6		(17, 5, 64)	5.00
R Superior Frontal Gyrus BA 8		(18, 17, 52)	5.20
L Superior Frontal Gyrus BA 6		(-22, 7, 46)	5.20
L Superior Frontal Gyrus BA 8		(-27, 14, 56)	5.44
L Parietal Sub-Gyral BA 40		(-25, -42, 60)	4.24
L Postcentral Gyrus BA 3		(-17, -43, 72)	5.04
L Cingulate Gyrus BA 24		(-9, -10, 34)	4.75
Left hemisphere			
Frontal			
Frontal Sub-Gyral	11730	(-31, 45, 1)	5.55
Frontal Sub-Gyral Corpus Callosum		(-16, 38, 0)	4.78
Inferior Frontal Gyrus BA 47		(-28, 29, -9)	6.44
Medial Frontal Gyrus BA 10		(-11, 56, 7)	4.58
Middle Frontal Gyrus		(-44, 41, 0)	4.35
Middle Frontal Gyrus BA 10		(-30, 54, -9)	4.42
Inferior Frontal Gyrus BA 45	1768	(-46, 22, 9)	5.29
Medial Frontal Gyrus BA 8		(-6, 34, 40)	4.83
Medial Frontal Gyrus BA 9		(-4, 45, 29)	4.13

	1935		
Superior Frontal Gyrus BA 9		(-15, 47, 24)	5.37
Precental Gyrus BA 4	2846	(-50, -10, 21)	3.95
Precentral Gyrus BA 4		(-47, 2, 16)	4.69
Frontal, Parietal			
Frontal Sub-Gyral	2423	(-39, -22, 22)	4.31
Inferior Parietal Lobule BA 40		(-45, -31, 31)	5.12
Midbrain, Subcortical			
Midbrain	9431	(-12, -22, -6)	4.39
Corpus Callosum		(-8, -32, 1)	4.93
Extra-Nuclear		(-34, -6, -4)	4.78
Lateral Globus Pallidus		(-11, 8, -3)	4.27
Thalamus Medial Dorsal Nucleus		(-11, -20, 8)	5.51
Thalamus Ventral Lateral Nucleus		(-9, -8, 7)	7.38
Occipital			
Cuneus BA 18	421	(-10, -70, 15)	4.51
Parietal, Cingulate			
Parietal Sub-Gyral	6539	(-27, -54, 30)	5.51
Precuneus BA 7		(-10, -63, 36)	4.84
Cingulate Gyrus BA 31		(-20, -70, 18)	3.97
		(-14, -51, 25)	4.09
Temporal			
Middle Temporal Gyrus BA 22	2869	(-54, -41, -1)	6.29
Superior Temporal Gyrus BA 22		(-56, -54, 20)	4.69
Superior Temporal Gyrus BA 39		(-51, -51, 9)	3.90
Superior Temporal Gyrus BA 22	1349	(-53, -20, -3)	4.92
Right hemisphere			
Frontal			
Frontal Sub-Gyral	713	(35, 13, 26)	5.46
Superior Frontal Gyrus BA 8	474	(17, 34, 38)	4.25
Frontal, Temporal			
Precentral Gyrus BA 4	6857	(59, -5, 19)	4.22
Precentral Gyrus BA 44		(51, 1, 4)	5.57
Precentral Gyrus BA 6		(49, -1, 27)	3.99
Fusiform Gyrus BA 20		(58, -12, -32)	5.60
Middle Temporal Gyrus BA 21		(56, -13, -20)	5.43
Superior Temporal Gyrus BA 22		(59, -9, -6)	4.76
Midbrain, Subcortical			
Midbrain	6096	(16, -9, -9)	4.53
Thalamus Pulvinar		(19, -21, 7)	6.48
Thalamus Ventral Anterior Nucleus		(10, -5, 5)	5.73
Parietal, Cingulate			
Precuneus BA 7	2194	(14, -55, 56)	4.80
Superior Parietal Lobule BA 7		(19, -50, 68)	3.81
Cingulate Gyrus BA 31		(10, -46, 35)	4.06
Posterior Cingulate BA 23		(3, -52, 20)	4.57
Parietal, Temporal			
Inferior Parietal Lobule	1596	(43, -45, 22)	4.60
Supramarginal Gyrus BA 40		(53, -52, 23)	4.99
Parietal, Temporal, Occipital, Subcortical			
Angular Gyrus BA 39		(44, -66, 30)	5.08
Parietal Sub-Gyral		(27, -51, 40)	4.37

		7117		
	Precuneus BA 31		(17, -63, 32)	3.74
	Superior Parietal Lobule BA 7		(30, -59, 58)	4.78
	Supramarginal Gyrus BA 40		(38, -53, 33)	4.49
	Superior Temporal Gyrus BA 22		(41, -57, 18)	3.86
	Temporal Sub-Gyral		(26, -61, 15)	5.02
	Superior Occipital Gyrus BA 19		(13, -76, 31)	4.48
	Corpus Callosum		(18, -52, 21)	4.43
Temporal				
	Middle Temporal Gyrus BA 20	1311	(58, -35, -21)	5.26
	Middle Temporal Gyrus BA 21		(62, -32, -9)	4.88
	Superior Temporal Gyrus BA 42	1500	(61, -33, 15)	5.17

Table D.6: Cluster peaks and subpeaks for the main effect of race. Positive T-values indicate that ^{18}F-AV-1451 SUVR is greater among black compared to non-black individuals.

	Label	Volume (mm^3)	MNI (x, y, z)	T-value
Bilateral				
Frontal				
	R Middle Frontal Gyrus BA 6	13235	(33, 2, 58)	5.77
	R Superior Frontal Gyrus BA 6		(8, 22, 61)	5.31
	R Superior Frontal Gyrus BA 8		(20, 19, 50)	4.90
	L Superior Frontal Gyrus BA 8		(-10, 37, 54)	4.66
	L Superior Frontal Gyrus BA 9		(-12, 60, 33)	3.74
Left hemisphere				
Cerebellum				
	Anterior Lobe	826	(-17, -42, -37)	4.23
		420	(-27, -47, -39)	4.77
Frontal				
	Middle Frontal Gyrus BA 46	1371	(-41, 28, 22)	4.29
	Middle Frontal Gyrus BA 9		(-41, 35, 32)	4.94
	Middle Frontal Gyrus BA 6	959	(-34, 9, 62)	4.88
Occipital				
	Cuneus BA 17	1358	(-19, -73, 22)	5.14
	Cuneus BA 18		(-3, -74, 14)	3.78
		755	(-8, -74, 2)	4.13
	Lingual Gyrus BA 18		(-17, -74, -9)	4.76
	Middle Occipital Gyrus BA 18	1855	(-32, -86, -1)	4.38
	Superior Occipital Gyrus BA 19		(-31, -84, 26)	4.54
Parietal				
	Precuneus BA 7	2368	(-5, -77, 42)	5.09
Subcortical				
	Thalamus Medial Dorsal Nucleus	862	(-11, -21, 10)	4.19
	Thalamus Pulvinar		(-23, -30, 6)	3.99
Right hemisphere				
Frontal				
	Precentral Gyrus BA 6	1236	(27, -20, 71)	4.95
Occipital				
	Cuneus BA 17	2669	(16, -89, 2)	4.66
	Lingual Gyrus BA 17		(8, -91, -10)	4.92
	Lingual Gyrus BA 18		(9, -79, -2)	3.93
	Lingual Gyrus BA 19		(18, -67, -4)	5.11
	Middle Occipital Gyrus BA 19	506	(28, -86, 12)	4.04
Temporal				
	Inferior Temporal Gyrus BA 20	890	(60, -17, -30)	4.36
	Middle Temporal Gyrus BA 21		(59, -13, -15)	5.49
	Middle Temporal Gyrus BA 20	514	(61, -39, -15)	4.94
	Parahippocampal Gyrus BA 27	531	(22, -30, -10)	4.70
Temporal, Midbrain				
	Parahippocampal Gyrus BA 28	415	(23, -20, -14)	3.73
	Midbrain		(9, -7, -9)	4.28

Appendix E. Entorhinal volume and mean ^{18}F-AV-1451 SUVR in Braak III/IV

Table E.1: Linear mixed effects models of the relationship between mean ^{18}F-AV-1451 SUVR in Braak III/IV regions and intracranial volume adjusted entorhinal cortex volume. Estimated fixed effects are reported along with their standard errors in parentheses.

	Dependent variable: Regional volume (cm^3)
	Entorhinal volume
Intercept	-0.310^{***} (0.064)
	p = 0.000003
Age at PET scan	-0.033^{***} (0.007)
	p = 0.00004
Sex	0.467^{**} (0.142)
(ref = female)	p = 0.002
Amyloid group	0.287 (0.161)
(ref = amyloid–)	p = 0.083
Braak III/IV SUVR	-1.634^{*} (0.804)
	p = 0.049
Time from PET	-0.056^{***} (0.007)
	p = 0.000
Amyloid group	0.002 (0.018)
× time	p = 0.900
Braak III/IV SUVR	−0.034 (0.085)
× time	p = 0.687
Note:	*p<0.05; **p<0.01; ***p<0.001

Appendix F. Cognition and tau accumulation

Table F.1: Linear mixed effects models of the relationship between mean ^{18}F-AV-1451 SUVR in Braak III/IV regions and attention. Estimated fixed effects are reported along with their standard errors in parentheses.

	Dependent variable: Attention (z-score)
Intercept	0.114 (0.093) p = 0.219
Age at PET scan	−0.026* (0.010) p = 0.014
Sex (ref = female)	0.017 (0.195) p = 0.932
Education (years)	0.019 (0.043) p = 0.653
Amyloid group (ref = amyloid–)	0.255 (0.247) p = 0.307
Braak III/IV SUVR	−2.463* (1.121) p = 0.033
Time from PET	−0.020*** (0.006) p = 0.0005
Amyloid group × time	−0.022 (0.017) p = 0.206
Braak III/IV SUVR × time	0.045 (0.062) p = 0.475
Note:	*p<0.05; **p<0.01; ***p<0.001

Table F.2: Linear mixed effects models of the relationship between mean ^{18}F-AV-1451 SUVR in Braak V/VI regions and attention. Estimated fixed effects are reported along with their standard errors in parentheses.

	Dependent variable: Attention (z-score)
Intercept	0.123 (0.092) p = 0.184
Age at PET scan	-0.026^{*} (0.010) p = 0.016
Sex (ref = female)	0.051 (0.213) p = 0.811
Education (years)	−0.019 (0.047) p = 0.692
Amyloid group (ref = amyloid–)	0.247 (0.238) p = 0.305
Braak V/VI SUVR	-2.033^{*} (0.885) p = 0.027
Time from PET	-0.016^{**} (0.006) p = 0.004
Amyloid group × time	0.001 (0.017) p = 0.945
Braak V/VI SUVR × time	−0.063 (0.040) p = 0.118
Note:	*p<0.05; **p<0.01; ***p<0.001

Table F.3: Linear mixed effects models of the relationship between entorhinal ^{18}F-AV-1451 SUVR and California Verbal Learning Test (CVLT) z-scores. Estimated fixed effects are reported along with their standard errors in parentheses.

	Dependent variable: CVLT (z-score)	
	Immediate recall	Long-delay free recall
Intercept	0.105 (0.122) p = 0.391	0.146 (0.132) p = 0.269
Age at PET scan	−0.032* (0.012) p = 0.011	−0.027* (0.013) p = 0.042
Sex (ref = female)	−0.101 (0.214) p = 0.641	−0.037 (0.230) p = 0.875
Education (years)	−0.089 (0.051) p = 0.084	−0.047 (0.054) p = 0.397
Amyloid group (ref = amyloid–)	0.127 (0.302) p = 0.677	0.122 (0.326) p = 0.711
Entorhinal SUVR	−0.645 (0.924) p = 0.489	−0.893 (0.996) p = 0.375
Time from PET	−0.024*** (0.006) p = 0.0001	−0.022*** (0.006) p = 0.0005
Amyloid group × time	0.011 (0.015) p = 0.480	0.001 (0.015) p = 0.965
Entorhinal SUVR × time	−0.078 (0.041) p = 0.060	−0.095* (0.042) p = 0.024
Note:	*p<0.05; **p<0.01; ***p<0.001	

Table F.4: Linear mixed effects models of the relationship between mean ^{18}F-AV-1451 SUVR in Braak III/IV regions and California Verbal Learning Test (CVLT) z-scores. Estimated fixed effects are reported along with their standard errors in parentheses.

	Dependent variable: CVLT (z-score)	
	Immediate recall	Long-delay free recall
Intercept	0.102 (0.123) p = 0.407	0.143 (0.132) p = 0.281
Age at PET scan	−0.032* (0.012) p = 0.011	−0.027* (0.013) p = 0.045
Sex (ref = female)	−0.102 (0.228) p = 0.658	−0.074 (0.245) p = 0.763
Education (years)	−0.085 (0.050) p = 0.099	−0.045 (0.054) p = 0.413
Amyloid group (ref = amyloid–)	0.215 (0.324) p = 0.511	0.241 (0.349) p = 0.494
Braak III/IV SUVR	−1.179 (1.466) p = 0.426	−1.566 (1.581) p = 0.328
Time from PET	−0.025*** (0.006) p = 0.0002	−0.023*** (0.006) p = 0.0004
Amyloid group × time	0.018 (0.018) p = 0.319	0.015 (0.018) p = 0.390
Braak III/IV SUVR × time	−0.091 (0.074) p = 0.220	−0.163* (0.073) p = 0.026
Note:	*p<0.05; **p<0.01; ***p<0.001	